a steeply decreasing pressure gradient over the convergent section of a meter, and thus the laminar layer is preserved. On the other hand an increasing or 'adverse' pressure gradient operates over the diverging portion which causes instability in the boundary-layer flow over the pressure transition stage in the vicinity of the throat; a laminar boundary-layer at entrance to a meter is probably triggered to a turbulent one in the venturi throat and this transition, or absence of it, affects the discharge coefficient C_d appreciably.

One important feature of venturi meter flow would be decisive in determining whether a throat boundary-layer is laminar or turbulent: It can be shown experimentally that at entrance to a meter - in the region of curvature change at the junction of a cylindrical pipe and a conical meter - the pressure rises steeply. This adverse pressure gradient tends to trigger the unstable laminar boundary-layer at entrance to a meter. Separation bubbles could be formed prior to re-attachment of the boundary-layer in turbulent or laminar-turbulent form. Such a boundary-layer would probably be wholly turbulent in the throat due to the pressure transition outlined earlier. On the other hand it is clear that a laminar boundary-layer could exist in a venturi throat - depending on meter geometry and flow conditions - if, for example,

the layer is not triggered at entrance to a meter.

In the light of the above considerations, the author proposes to estimate the effect of this boundary-layer factor assuming the throat boundary-layer is either laminar or turbulent. Further, the semi-infinite flat plate analogy will be employed, taking the effective length for boundary-layer development as $\ell = 1.3\ d$, as suggested by Hutton,[87] instead of $\ell = d$ as used by Hall.[1] It is proposed to calculate the throat displacement thicknesses which will modify the area ratio, m, and hence C_d.

In conclusion it needs to be emphasized, however, that Hutton's expression for C_d showed negligible changes in C_d for small variations in m.

3.5 The impact pressure effect

The pressure in the corner of the upstream side of a venturi contraction is higher than that, say, one pipe diameter upstream from it. As the fluid enters the converging cone, the stream lines are bent inwards; this 'squeezing' of stream tubes causes energy losses which give rise to a decrease in axial momentum of the fluid. The momentum loss, in turn, causes a reaction force at entrance to the converging cone which increases the differential pressure above the true value.

This 'impact pressure' has been measured by Engel and Witte [92] who suggested a theoretical approach for calculating the pressure. Their mathematical treatment is vague and unconvincing, however, particularly where they introduce an undefined constant of proportionality for determining the impact pressure coefficient. The effect of the converging cone angle was neglected in spite of the fact that the degree of convergence is known to affect the induced impact pressure markedly.

It is possible to calculate the force imposed on the projected cone surface by the abovementioned change in axial momentum and the resulting impact pressure can be considered as proportional to the pressure caused by this force or,

$p_i = K p_f$, where p_i is the impact pressure and p_f the pressure caused by the momentum change reaction force. The constant K would depend on ϕ_1, m, and f, where ϕ is the angle of convergence, f_1 the internal cone friction coefficient, and m the area ratio of the meter. The determination of p_f is based on Newton's second law which would not be applicable if separation were to take place upstream of the contracting section. This will be referred to further on when the effect of separation is dealt with.

In an attempt to allow for the effect of this factor - which has been ignored by most investigators in the past - the author has developed a theoretical expression for p_f, and evaluated the impact pressure coefficient.

3.6 The effect of losses through the venturi meter

This is yet another controversial factor. The losses through a conical meter are composed of : the boundary resistances in a pipe of length $\frac{D}{2}$, in the conical contraction, and in a throat length of $\frac{d}{2}$. Rigorous mathematical treatment is complicated. Apart from curvature, eddying and possible separation losses, the velocity varies with length and the coefficient of friction varies with velocity. The effects of pressure gradients and boundary-layer growth in the converging cone further complicate the analysis.

Pordoe [97] suggested an empirical formula for determining these losses viz :

$K_L = \frac{0.0435}{d^4}$, where d represents the throat diameter in inches. The above formula can be written as :

$$K_L = \frac{K}{d^n} \qquad \ldots\ldots\ldots\ldots\ldots\ldots\ldots\ldots (6.2)$$

where K is a constant.

If the constant in equation (6.2) takes care of friction coefficient, area ratio, angle of convergence

etc., K would vary for different meters but equation (6.2) would suffice provided that K could be determined as a function of these factors. In the above form, however, it cannot be applied to a particular meter since K_L is not a function of the throat diameter only, while K is a complex function of f, n, β, and the general internal geometry.

Hutton (87) developed the relationship :

$$K_L = f\frac{x}{d} \qquad \ldots\ldots\ldots\ldots\ldots\ldots\ldots\ldots (6.3)$$

He treated the entire nozzle loss as being analogous to that in an equivalent pipe of length x and diameter identical to the venturi throat diameter, d. Hutton also assumed that friction and kinetic losses could be included in one friction coefficient, f. His analysis of experimental data for meters having an effective internal roughness size of $\epsilon = 0.0022$ showed that $\frac{x}{d}$ can be taken as approximately 2, yielding :

$$K_L = 2f \qquad \ldots\ldots\ldots\ldots\ldots\ldots\ldots\ldots (6.4)$$

This formula, when applied to practical tests, gave good agreement with experimental results. A few points of criticism should however be noted : Hutton assumed the flow in the throat to be fully developed whereas it is not. The author is of the opinion that

this erroneous assumption does not affect the validity of equation (6.4) because the difference between the actual and assumed fully developed flow conditions can be accounted for in the choice of the empirical value $\frac{K}{d}$ which is in fact determined from experimental data.

Hutton dealt with roughness, friction and area ratio effects but neglected the effect of the angle of convergence. Effects due to boundary-layer growth and pressure gradients were also ignored although it could be argued that the empirical value of $\frac{K}{d}$ would probably look after these influences.

The author attempted to derive an expression for K_L based on the same principle as that applied for determining the impact pressure. By considering the change in axial momentum between the upstream and downstream tapping sections, the total loss through the venturi could probably be expressed by $K_L = K' p_T$, where p_T is the pressure due to the axial momentum change. The resulting relationship gave values for K_L which agreed exactly with those obtained from Hutton's formula for the classical venturi meter tested ($n = 0.25$), but the author's formula did not apply to meters of larger area ratios.

Guided by the above considerations, the author

decided to use the Hutton formula in allowing for the overall loss factor since his relationship, although not comprehensive, recognises the effects of major import.

3.7 The static pressure error effect

This error is caused by two separate factors : An error is introduced due to the pipe wall static pressure hole size and, in the second place, because of turbulence, even this corrected wall static pressure would be in excess of the true average static pressure over the pipe cross-section.

The influences of these factors were analysed comprehensively in Chapter IV to which the reader is referred for detail.

It is surprising to report that, apart from brief references to their possible existence, the author could not find any evidence of attention having been paid to the effects of these two factors in analytical or experimental work. When it is considered that painstaking corrections are made in the laboratory for such factors as water temperature, density, buoyancy of air in discharge measurement, weight and temperature of air in compressed air-water manometers, and the value of π, it is remarkable that static pressure and turbulence correction factors are neglected. The following static

pressure corrections are suggested.

3.7.1 Static pressure correction for hole-size

This correction is given, for different values of $\frac{d_s}{D}$ and Reynolds number, in Fig. 4.3 of Chapter IV. Here d_s = static pressure hole diameter and D = pipe diameter. The correction will be denoted by Δ_p^h, or $p_{w1} = p_1 + \Delta_p^h$, where p_{w1} represents the wall static pressure corrected for hole size.

3.7.2 Average static pressure correction due to turbulence

The magnitude of this correction is given by $\overline{\Delta}_p' = 1.26\ T_s$ as shown in Fig. 4.9 of Chapter IV. Thus, the true static pressures are :

$$\overline{p}_{s1} = p_{w1} - 1.26\ T_s \quad \text{at the upstream, and} \quad \ldots\ (6.5)$$

$$\overline{p}_{s2} = p_{w2} - 1.26\ T_s \quad \text{at the throat sections} \quad \ldots\ (6.6)$$

The effects of these factors can therefore be evaluated and corrected for as shown later.

3.8 The effect of turbulence

Because of lack of experimental data on turbulence at entrance to and in a venturi throat at different

Reynolds numbers, the effect of this factor has till now been neglected. If such data were available, the necessary corrections could be made by including a turbulence term in the fundamental Bernoulli equation.

Thus, the total energy at, say, the upstream tapping section would be expressed by :

$$\bar{e}_1 = \bar{P}_{s1} + \tfrac{1}{2}\lambda_1 \rho \overline{v_1^2} + \tfrac{1}{2}\rho(\overline{v_1'^2} + \overline{u_1'^2} + \overline{w_1'^2}) \quad \ldots\ldots\ldots\ldots\ldots\ldots (6.7)$$

where $\bar{P}_{s1}$ = true static pressure.

λ_1 is the upstream velocity distribution correction factor and

$\tfrac{1}{2}\rho(\overline{v_1'^2} + \overline{u_1'^2} + \overline{w_1'^2})$ is the turbulence correction term.

By correcting the total pressure in the throat section in a similar manner, a theoretical expression for the discharge coefficient can be derived - as will be shown further on - in which this factor effect features.

Extensive further experimental work on r.m.s. values of turbulent velocity fluctuations in venturi meters is, however, imperative before this effect can be fully evaluated.

3.9 The effect of rounded upstream and throat corners

Rounded corners joining a converging cone to an upstream pipe or throat section seem to affect the 'hump' sometimes found in meter characteristics. It also influences throat boundary-layer growth.

Schlag [98] reported that the 'hump' tends to decrease and even to disappear completely when the cone is joined to the upstream pipe and/or throat by means of fillets of large radii ($r = 2D$). The peculiar dip sometimes found in meter characteristics at low Reynolds numbers, as reported by Schlag in reference (21), is attributable to the separation of flow caused by deceleration in the peripheral stream lines. He states that this is particularly evident when the radii at the outlet of the convergent cone are large. The same author also reports an increase in C_d at large Reynolds numbers due to a radius at the outlet of the convergent cone.

The throat radius should counteract separation at entry to the throat at high Reynolds numbers and because of the effect on boundary-layer growth in the throat would influence C_d. Little published data on this influence are available.

The ASME Research Committee [56] specifies fillet radii identical to those proposed by the International

Standards Organisation. The radius between a pipe and convergent cone is given as between zero and 1.375 times the pipe diameter, while that between a convergent cone and the throat is specified to lie between $3\frac{1}{2}$ and $3\frac{3}{4}$ times the throat diameter. Schlag [98] recommended a radius of 2D in order to get rid of the 'hump' but subsequently stated that he was opposed to radiussing on account of manufacturing difficulties.

Rounding the entrance and throat corners would probably ensure a laminar throat boundary-layer at fairly high Reynolds numbers; this could be the cause of the steady increase in C_d with Reynolds number if Hall's boundary-layer theory is correct.

Witte [109] found that the effect of these radii on C_d was quite marked; radiussing would therefore be advantageous provided it could be standardised and controlled.

To determine the exact effect of this factor, the author suggests that a series of experiments be carried out, using fillets of different radii, in which experimentally determined C_d-values could be correlated with fillet radii, resulting pressure gradients, and boundary-layer growth.

3.10 The effects of upstream and throat tapping positions and throat length

On a classical venturi meter, the upstream tapping point is located at a distance $\frac{D}{2}$ upstream from the inlet to the convergent cone. Schlag [98] experimented on venturi meters having dimensions D = 100 mm and d = 50 mm, with different degrees of roughness in the upstream pipe and convergent cone. The position of the upstream tapping point was varied from approximately 49.75 ($\frac{D}{2}$) to 29.25 and 12.2 mm from the convergent cone inlet. He reported that these different positions had no effect on the discharge coefficient. The author is of the opinion that, provided a tapping is not located in the upstream corner, no effect should be noticeable. In the corner the pressure would be affected not only by curvature of streamlines but also by impact pressure.

Schlag [98] also experimented on the effect of throat tapping position. He used the abovementioned venturi meter with throat lengths of 30, 25, 20 and 15 mm, locating the tapping point 8 mm downstream from the entrance to the throat. The difference between C_d-values for convergent cone angles of 10° and 20° was, with one exception, below 0.5 per cent and in some cases it was negligible.

The author is of the opinion that if a throat tap

is positioned at either end of the throat length, pressure would be affected by curvature of streamlines and throat boundary-layer growth. However, at any distance in between where boundary-layer development has taken place, the tapping position should not affect a pressure reading. It is also evident that the throat length does not influence C_d.

3.11 The internal meter roughness effect

It is known that increased roughness of a convergent cone causes C_d to decrease.

Schlag [98] carried out experiments on a venturi meter identical to the one referred to above. The internal surface of the cone was progressively covered with a thin coat containing more than 50 per cent Cu_2O, and the meter was successively tested with a 'smooth' and 'r[illegible]' upstream pipe. The effect on C_d proved considerable and it was shown that smooth convergent cones were very easily soiled. He also reported that cast-iron cones show a more pronounced discrepancy than brass convergent cones in the clean and soiled condition, respectively.

Spencer and Thibessard [2] found that differences in C_d due to increased meter roughness diminished with decreasing Reynolds numbers down to 2×10^5. This

result is of the utmost importance for future experimental and analytical work. It suggests a similarity to normal pipe flow in that the inverted forms of meter characteristic curves of C_d vs R_e, for different internal meter roughness, seem to be identical in form and shape to the normal type of pipe-friction chart or Nikuradse curves. If similarity or a definite relationship could be established, it would constitute a major break-through in this field.

In reference (2), the authors state that : 'If this similarity in flow mechanism is verified then a method of predicting the entire characteristic from a knowledge of the original characteristic, and the state of the meter at any time, becomes practicable'. Further research in this direction should be of great value.

If internal roughness changes are caused by accumulation of surface deposits, the roughness would also influence internal pipe and throat diameters. The changes in C_d resulting from the use of inaccurate diameter measurements are given as : (2)

For a throat diameter error of Δd, percentage change in $C_d = \left(\frac{2}{1 - m^2}\right) \frac{\Delta d}{d}$, and for a pipe diameter error

of Δ_D, percentage change in $C_d = \left(\frac{2m^2}{1-m^2}\right) \cdot \frac{\Delta D}{D}$

Test on a 6 inch, 0.25 area ratio venturi meter with internal rust at N.E.L. showed that application of the above correction factors reduced a possible error of 1.0 per cent to one of the order of 0.3 per cent. It can be shown that the pipe and throat diameters must be measured to within $\pm$ 0.1 and $\pm$ 0.02 per cent respectively to keep the error due to this influence to within tolerable limits.

It is evident that the change in C_d resulting from use and age is directly related to variation of internal meter roughness caused by internal deposits, grit formation or soiling.

The problems associated with internal roughness were outlined very clearly by Hayward in his discussion of reference 2. He stated that 'if a venturi meter was used to cultivate moss' a $\frac{1}{4}$ per cent loss of accuracy was quite understandable. At N.E.L. where the laboratory water was flocculated, filtered and treated, there was a change of $\frac{1}{4}$ per cent in C_d after a venturi meter was left in a line for only three weeks. In industrial applications, therefore, a user of venturi meters would not be able to rely on even the second decimal place given for C_d in the calibration certificate after the meter had been in

use for some time.

The first comprehensive analysis of the roughness problem was made by Hutton [87] who suggested a reasonable semi-empirical method for estimating reliable values for C_d after a number of years of meter use.

The author suggests that future experiments to yield a series of observed effects on C_d resulting from changes in internal meter roughness would not contribute to a better understanding of the problem. Rather, the example set by Hutton [87] and Hall [1] should be followed. For different meter sizes and/or roughness, experimental C_d values should be related to entrance and throat velocity profiles, total meter losses, convergent cone and throat boundary-layer characteristics, impact pressure, static pressure corrections and turbulence structure, in an attempt to correlate separately these effects on C_d. The author has derived a theoretical expression for C_d which might be of assistance in such an experimental programme. This is dealt with further on.

3.12 The effect of rounding the inside edges of the pressure tapping holes

The effect of this factor on static pressure measurement was dealt with in detail in Chapter IV. Some authorities advocate a 'slight' radiussing of the

internal edge while others are of the opinion that this would not improve the accuracy of static pressure measurement.

Work at Liverpool University [17] indicates that a 'slight' radiussing of one-tenth the tapping hole diameter is advantageous, while the ASME code prescribes radii which do not seem to have any relationship to hole diameter.

In Chapter IV, the author suggested the lines of further investigations to define more precisely the influence of this factor.

3.13 The effect of the angles of contraction and diffusion

In a test series on identical venturi meters having angles of convergence of 12 degrees and 15 degrees respectively, Schlag [98] found that meters with 12 degree cones gave discharge coefficients consistently 1 to 2 per cent higher than those for 15 degree convergence. He also showed that the overall losses for the meter having a 15 degree cone were higher than those for the meter with 12 degree convergence.

The former result can be explained by the fact that the larger contraction angle would cause a higher differential pressure to be registered, due to a higher

impact pressure, and therefore the 15 degree meter would have a smaller coefficient than the 12 degree one.

It is clear that overall losses would be higher for the meter with the larger convergence angle due to a higher degree of contraction.

In reference 98 Schlag reported that in tests on meters having 10 degree and 20 degree angles of divergence, no effect on C_d could be detected but, as could be expected, the overall meter loss was higher for the latter because the more gradual the diffusion, the smaller the energy loss.

In his discussion of the paper in reference 17, Hooper expressed the opinion that a divergence angle in excess of 12 degrees was liable to cause separation depending on the turbulence level in the upstream flow, roughness effects, etc. He found that when the divergent cone was greasy the flow tends to separate at high angles of divergence.

Contributing to Schlag's paper, (98) Ruppel said they had found in Germany that the angle of divergence has only a slight effect on the meter coefficient, but that if the length between the throat pressure tap and the beginning of the diffuser was too short, there was a pronounced effect.

The author is of the opinion that mere observation and recording of different effects caused by changing the angle of convergence and divergence, as reported above, will not contribute much towards a solution of the problem. Correlation among the major effects influencing C_d must be sought experimentally but on a basis dictated by analysis and new hypothesis.

3.14 Effect of the method of pressure tapping

Static pressure tappings were dealt with in detail in Chapter IV. The most commonly employed methods comprise piezometer rings or a number of static pressure holes around the pipe circumference - usually four at the throat and six at the upstream section.

If piezometer holes or rings become soiled errors will arise and furthermore circulation in piezometer rings, due to turbulence, will also affect static pressure readings. Air trapped in these rings or annular grooves should be bled off.

The author is of the opinion that future development work on this factor should be concentrated on the static hole pressure correction as suggested and outlined in Chapter IV. In most practical applications, turbulent flow causes circulation in an annular groove or ring. To evaluate this effect seems to be a much more complex

problem than to refine the corrections to be made to a wall static hole pressure measurement. When a number of static pressure holes are linked by an external ring, circulation in this ring would be damped to a greater degree than that due to turbulence in an internal piezometer ring. Provision of static pressure holes around a circumference - correcting for hole size and turbulence - is therefore to be preferred to an internal piezometer ring or annular chamber.

3.19 Other factor influences

Other factors affecting the determination of C_d are : Differential pressure measurement and corrections, meter installation effects and temperature changes in the metering fluid. Reference 95 deals with these in detail and it is clear that elimination of errors due to these factors does not constitute a great obstacle because the mechanisms involved are well understood. Over-refinement in dealing with these errors would, however, be superfluous because of the overriding influences of the other factors discussed.

4. THEORETICAL ANALYSIS

In this section the author attempts to analyse theoretically the major factors affecting flow through a conical venturi meter in the light of the foregoing

factor analysis.

The fundamental relationship for a venturi meter is equation (6.1) which is derived from Bernoulli's Theorem - a simple one-dimensional application of the energy conservation principle. Many experimenters refer vaguely to some of these neglected factors without attempting a comprehensive theoretical analysis which would take account of the dominating factor effects.

The factors to be considered may be listed as follows :

4.1 Non-uniformity of velocity distribution outside the boundary-layer at entrance to a meter is to be evaluated by means of a coefficient λ_1.

4.2 Non-uniformity of velocity distribution outside the boundary-layer at a venturi throat is to be evaluated by means of a coefficient λ_2.

4.3 Venturi nozzle losses due to the shape and roughness is to be accounted for by a coefficient K_L.

4.4 Impact pressure caused by inward bending of stream filaments in a contracted passage is to be corrected for by a factor β operating on the differential pressure Δ_p.

4.5 The effect of boundary-layer growth and throat

boundary-layer influence will be considered by assuming that the effective throat radius is decreased by an amount equal to the boundary-layer displacement thickness which alters m, the area ratio.

In the first place, a theoretical expression is derived, expressing C_d as a function of the above factor effects. Theoretical and experimental results are compared.

In the next step, three additional factors are considered and a relationship is suggested for calculating C_d from experimental results in future research. These factors are the following :

4.6 The effect of static pressure correction due to static hole size.

4.7 The effect of average static pressure correction due to turbulence.

4.8 The effect of total energy correction due to turbulence.

4(A) Derivation of first expression for C_d

Kinetic energy coefficient, λ_1, affects the average velocity at entrance V_1; λ_2 and K_L influence the throat velocity V_2, and β affects the pressure differential Δ_p.

Adjustment of the conventional energy relationship for an incompressible fluid, neglecting turbulence yields :

$$P_{s1} + \frac{\lambda_1 \rho V_1^2}{2} = P_{s2} + \frac{\lambda_2 \rho V_2^2}{2} + \frac{K_L \rho V_2^2}{2}$$

$$\text{or } \beta(P_{s1} - P_{s2}) + \frac{\lambda_1 \rho V_1^2}{2} = \frac{\rho V_2^2}{2} (\lambda_2 + K_L) \quad \ldots\ldots(6.8)$$

The equation of continuity gives :

$$V_1 = \frac{\lambda_2}{\lambda_1} V_2 ,$$

$$\text{or } V_1^2 = \left(\frac{\lambda_2}{\lambda_1}\right)^2 V_2^2 = m^2 V_2^2 \quad \ldots\left(m = \frac{\lambda_2}{\lambda_1}\right)$$

Equation (6.8) therefore yields :

$$\beta(P_{s1} - P_{s2}) = \frac{\rho V_2^2}{2} (\lambda_2 + K_L - \lambda_1 m^2)$$

$$\text{or } V_2^2 = \frac{2 A_p \beta}{\rho(\lambda_2 + K_L - \lambda_1 m^2)} \quad \ldots\ldots (P_{s1} - P_{s2} = A_p)$$

$$\text{whence } Q = A_2 V_2 = A_2 \sqrt{\frac{\frac{2}{\rho} \cdot A_p \beta}{\lambda_2 + K_L - \lambda_1 m^2}}$$

$$\text{or } Q = \frac{A_2}{\sqrt{\lambda_2 + K_L - \lambda_1 m^2}} \cdot \sqrt{\frac{2}{\rho} \cdot A_p \beta} \quad \ldots(6.9)$$

Comparing equations (6.9) with the conventional equation (6.1) viz :

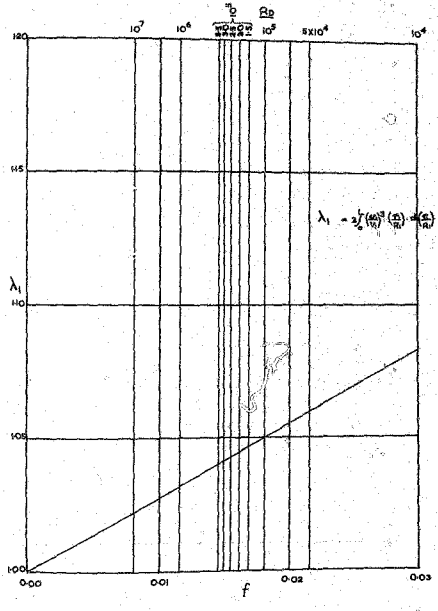

FIG. 6·1 FACTOR λ_1

$$Q = \frac{C_d A_2}{\sqrt{1 - m^2}} \cdot \sqrt{\frac{2}{\rho} \cdot h_p} \quad \text{yields :}$$

$$C_d = \sqrt{\frac{\beta (1 - m'^2)}{\lambda_2 + K_L - \lambda_1 m^2}} \qquad \ldots\ldots\ldots\ldots\ldots\ldots (6.10)$$

where m' is the altered area ratio due to the boundary-layer displacement thickness.

Equation (6.10) suggests that it might be possible to predict C_d theoretically if, for certain known conditions, the values of λ_1, λ_2, K_L, β and m' can be evaluated.

In Appendix V the theoretical analysis of the above factors has been treated in detail from first principles and appropriate expressions have been derived; evaluation of these (also dealt with in the Appendix) gave the following results :

$\lambda_1 = 1 + 2.93\, f - 1.55\, f^{3/2}$. This relationship is given in graphical form in Fig. 6.1.

$\lambda_2 = 1.00$, which is normal for a flat throat velocity profile. This value was checked by calculation;

$K_L = 2f$, according to Sutton's analysis. (87) The author revaluated this result;

β varies from 0.9882 for $f = 0.011$ to 0.9885 for $f = 0.03$, for the conical-type venturi meter tested.

This result was determined from the author's theory and Witte's and Engel's [93] experimental findings.

Values for m' were calculated for laminar and turbulent flows in a boundary-layer; m'_t for turbulent and m'_e for laminar flow.

It was now possible from equation (6.10) to calculate theoretical C_d values for various coefficients of friction and Reynolds numbers. Results are shown in Table V.I. It is important to note that equation (6.10) yields C_d-values which are identical for laminar and turbulent boundary-layer conditions. This result prompted the idea that possibly the boundary-layer or some other factor was overweighted in equation (6.10). On analysing the individual factors in equation (6.10) the author arrived at the conclusion that the theoretical concept and evaluation of β suggest that overall losses over a venturi meter are accounted for by this impact factor. It is clear that overall losses cause a differential pressure in excess of the true value and hence Hutton introduced the correction factor K_L. On the other hand the β-factor also corrects a measured differential pressure which is too high due to the impact pressure effect on the upstream pressure reading, and losses in the contraction. The author is therefore of the opinion that if β is introduced in the form suggested,

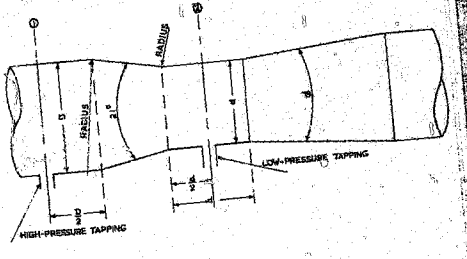

FIG. 6·2 HERSCHEL OR CONICAL VENTURI TUBE.

K_L should be discarded.

The resulting expression for C_d can therefore be written as :

$$C_d = \sqrt{\frac{8(1 - m'^2)}{\lambda_2 - \lambda_1 m'^2}} \qquad \ldots\ldots\ldots\ldots\ldots\ldots (6.11)$$

The above equation yielded theoretical values for C_d, for various Reynolds numbers and coefficients of friction, as shown in Table V.1. The similarity between C_d- values for laminar and turbulent throat boundary-layer conditions is again apparent. These theoretical values will later be compared with experimental results.

5. EXPERIMENTAL INVESTIGATIONS

Under the guidance of Dr. A.E. Spencer, the author carried out extensive tests in the laboratories at N.E.L. on a 4-inch diameter conical venturi meter with an area ratio of m = 0.25. The meter is shown in Fig. 6.2.

5.1 Experimental technique and accuracies

It has been established that the determination of C_d in a laboratory to an accuracy of 2 per cent poses no major experimental problem. When accuracies to the order of 0.25 per cent or better are required, however, cali-

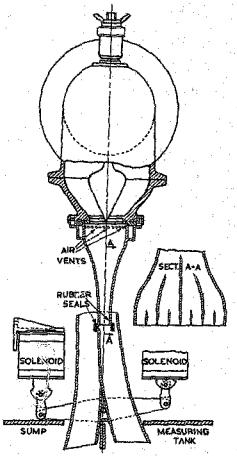

FIG.6·3 AUTOMATIC FLOW DIVERTER.

bration becomes a delicate operation. (95)

Results of tests carried out at N.E.L. revealed that accuracies to the order of 0.25 per cent require experimental techniques for measuring temperatures to 0.1°C, S.G. of the operating fluid (in this instance water) to at least 0.0001, the division time for determining flow rate to 0.01 seconds and the volume diverted to 0.02 per cent.

If the diverted flow is measured volumetrically the tank should be calibrated at regular intervals with the utmost care by weighing small quantities of water into the tank. The weighing machine should be sensitive to 1 part in 10,000; depth readings should be taken to an accuracy of approximately 0.01 per cent of total depth; buoyancy corrections are necessary, and a large number of points on the calibration curve should be taken for detection of possible deviations in the volume-height relationship. Temperature corrections should be made for the duration of the test and the tank should be sealed off to prevent evaporation.

Although flow rates are often measured volumetrically in tanks, the most accurate method is considered to be direct weighing of the diverted flow. (See Fig. 6.3)

A sufficient length of straight pipe in the cali-

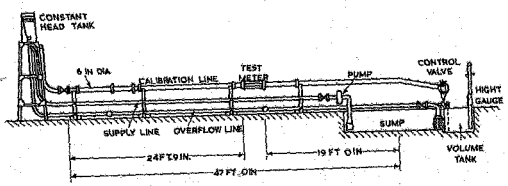

FIG. 6·4 FLOW METER CALIBRATION SYSTEM

bration rig must be provided both up- and downstream of the meter. The Test Code specifies 20 diameters upstream and 5 diameters downstream as a minimum. In the N.E.L. experiments the test lengths were increased to 42 diameters upstream and 15 diameters downstream of the meter. Before the meter is installed, it is important to ensure by pressure probe traverses at the particular sections that the flow is fully developed and that velocity profiles are symmetrical. Here, as in numerous other related experiments, pressure differential measurement is a familiar problem. At present it is believed that the ordinary U-tube manometer, using water-mercury, air-water, or other combinations, is more accurate than weigh-beam units or other devices. In the laboratory the miniscl can be read to 0.001 inches by means of a cathetometer, but the steady conditions necessary for this accuracy are seldom realised in the laboratory. Manometer fluctuations to the order of 0.001 of the differential at low flow rates, and as high as 0.005 of the differential at high flow rates, were encountered with undamped pressure leads. Flow straighteners and honeycombs were used in an attempt to improve the flow regime, but it was found that these precautions did not reduce fluctuations to any marked degree. The apparatus and experimental procedure are described in detail in reference (95). The calibration rig is shown in Fig. 6.4.

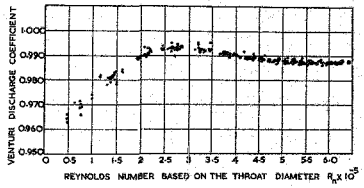

FIG-6-5 EXPERIMENTAL RESULTS ON 4-INCH VENTURIMETERS IN UPPER RE-RANGE

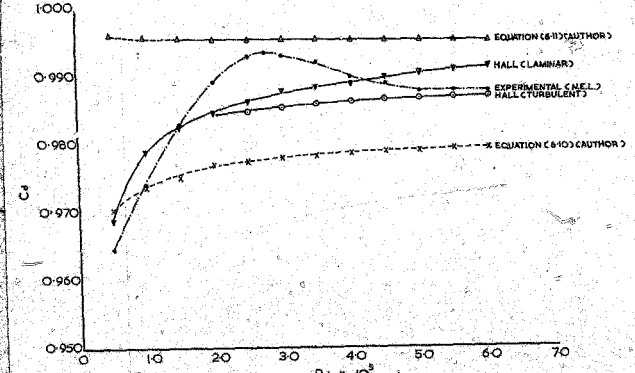

FIG. 6·6 INITIAL TESTS AT N.E.L.

5.2 Results

Experimental and theoretical coefficients of discharge were plotted against Reynolds numbers as shown in Figs. 6.5, 6.6 (See Table V.1 for theoretical values).

The author's theoretical values, according to equation (6.10) and (6.11) as well as Hall's results, have been included in Fig. 6.6. Hall's theoretical values are in good agreement with the experimental results. The graphs also show that the author's results, although not as good as Hall's, are in reasonable agreement when equation (6.10) is applied in the Reynolds number range up to approximately 1.5×10^5 and equation (6.11) in the range 2×10^5 and upwards. A transition zone seems to exist between these two Reynolds number values. Later tests were conducted on the same and identical venturi meters at the University of Liège and at N.E.L. It was reported [2] that the initial N.E.L. tests were carried out prior to internal cleaning of the meters with the result that there were discrepancies between the N.E.L. results given in Fig. 6.5 and the initial Liège results for an identical meter.

The results of the final N.E.L. and Liège tests are shown in Fig. 6.7. The author's theoretical values according to equations (6.10) and (6.11), together with

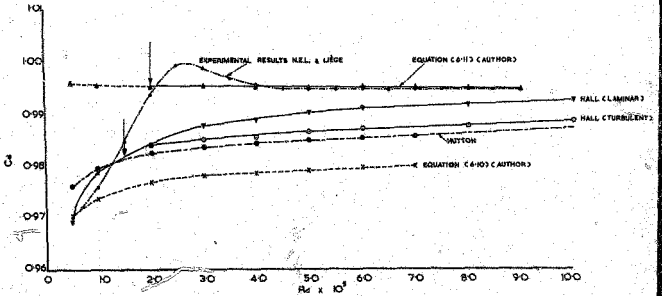

FIG.6-7 FINAL TESTS AT N.E.L. & LIÈGE

Hall's and Hutton's results have again been included in this figure. It is evident that Hall's values for a laminar boundary-layer are in better agreement with the experimental determinations than the author's results from equation (6.10) up to a Reynolds number of approximately 1.5×10^5. On the other hand, the author's values from equation (6.11) are in almost perfect agreement with the experimental findings at both N.E.L. and Liège in the Reynolds number range 2×10^5 and upwards.

Hall's values for laminar boundary-layer conditions show that C_d attains a constant value over the higher Reynolds number range, while turbulent conditions are associated with a steady increase of C_d. Equation (6.11) suggests a constant value of C_d for the higher Reynolds numbers.

The above results are now discussed in detail :

6. DISCUSSION OF RESULTS

As pointed out earlier, the experimental characteristic shown in Fig. 6.5 differed considerably from that obtained on an identical venturi meter tested at Liège. As subsequently reported,[2] this was because the N.E.L. meter had not been cleaned internally prior to testing. These results are therefore not used as a basis for comparison although the theoretical

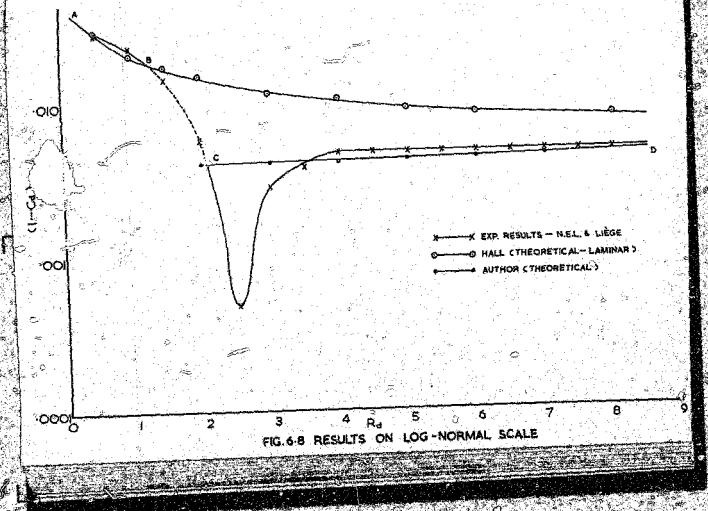

FIG. 6·8 RESULTS ON LOG-NORMAL SCALE

characteristics have been included as shown. The experimental characteristics of the final tests at N.E.L. and Liège [2] on identical meters agreed excellently and these are compared with theoretical determinations in Fig. 6.7. In Fig. 6.8 results are plotted on a log-normal scale to illustrate the resemblance to pipe friction curves.

The results show that :

6.1 The author's equation (6.10) yields a curve having the same general form as those given by Hutton's and Hall's solutions but lying further away from the experimental values. This, therefore, suggests no solution.

6.2 The author's equation (6.11) yields results which are in almost perfect agreement with experimental values in the Reynolds number range 2×10^5 and above.

6.3 Hutton's results and Hall's values for turbulent boundary-layer conditions are mutually in good agreement but both differ considerably from experimental values.

6.4 Referring to Fig. 6.8, Hall's results in the laminar range from A to B together with the author's theoretical values for the turbulent range from C to D represent the best agreement of theoretical with experimental determinations.

6.5 Experimental results plotted as shown in Fig. 6.8 show a close resemblance to pipe friction curves of a Moody diagram.

6.6 A continuous theoretical curve A B C D, assuming the dotted part through the transition stage, also bears a close resemblance to one of a family of pipe friction curves.

6.7 The 'hump' in the characteristics curve seems to disclose a feature omitted from the theoretical development because no theoretical solution fits the transitional and 'hump' stage. The results seem to confirm the author's arguments in the theoretical analysis that the impact factor β and the Loss-factor K_L, should not both be included in a theoretical relationship. In equation (6.11), β was introduced in favour of K_L and the results were in excellent agreement with experimental values over the turbulent range, and even in the 'hump' portion.

The author believed that a combination of Hutton's and Hall's theories, in a different or revised form, might hold the key to a theoretical solution, and accordingly adapted Hutton's general theory by introducing the β-factor. Clearly, any theoretical relationship for determining C_d-values should contain 'laminar', 'transitional' and 'turbulent' components and Hall's and the

author's equations offer a possible solution for the laminar and turbulent ranges.

The results further imply that a critical throat Reynolds number lies between 1.5×10^5 and 2.5×10^5. Below this range the coefficient appears to be dependent on Reynolds number and is unaffected by roughness, while above this critical range roughness and not Reynolds number seems to dominate C_d-values. If this hypothesis can be verified, a method of predicting complete meter characteristics from surface roughness measurements will follow.

Considering the theoretical graph A B C D (Fig. 6.8) it is clear that portion A B results from Hall's boundary-layer displacement thickness theory. The author's relationship $m_1' = m\,(1 - 3.945\,(R_e)^{-0.5})^2$ shows that the altered area ratio is a function of Reynolds number only; the roughness factor does not enter the picture. Because of very good agreement between experimental and theoretical values over part A B of the graph, it can be stated that below the critical Reynolds number C_d-values are dependent on Reynolds number only.

Now portion C D is defined by the author's equation :

$$C_d = \sqrt{\frac{\beta(1 - m'^2)}{\lambda_2 - \lambda_1 m'^2}} \qquad \ldots\ldots\ldots\ldots\ldots\ldots\ldots\ldots (6.11)$$

in which roughness factors predominate because λ_1, λ_2 and β are directly and/or indirectly related to the coefficient of friction. Furthermore, Table V.1 clearly shows that the displacement thickness or Reynolds number effect on the area ratio, m, leaves C_d unaffected when calculated for laminar and turbulent conditions by equation (5.11). The excellent agreement between experimental and theoretical values therefore allows the statement that, above the critical Reynolds number, C_d-values are dependent on roughness effects only and not on Reynolds number. Hence, the pipe friction curve hypothesis seems to have substantial theoretical justification in terms of Hall's and the author's equations.

Referring to Fig. 5.8 the three distinct zones A B, B C and C D can therefore be analysed as follows :

At entrance to a venturi meter it is assumed that the boundary-layer is laminar, as hypothesised earlier, having an unstable character due to adverse pressure gradients caused by curvature change. These pressure gradients trigger the laminar layer after entering the conical section resulting in separation at the critical Reynolds number. After re-attachment of the boundary-layer, transition sets in, in the form of a complex mixture of laminar and turbulent flow in the boundary-layer. At higher Reynolds numbers the boundary-layer

flow in the throat is wholly turbulent.

Thus, C_d-characteristics are related to laminar, transitional and turbulent zones, Reynolds number dominating the laminar zone while roughness effects control the turbulent zone as suggested by the theoretical analysis.

The hump in the characteristics-curve also can be explained in terms of the boundary-layer theory. When separation takes place after the laminar boundary-layer has broken up, the effective flow area at the separation section is decreased and consequently C_d has to increase for constant discharge through the meter. This C_d-value decreases accordingly after re-attachment of the boundary-layer. Should the position of separation move downstream with increasing Reynolds number, it could also cause a decrease in static pressure at the throat resulting in further lowering of C_d-values. Thus, a 'hump' could be formed in the transition zone.

The transition zone still remains theoretically undefined.

The influence of free-stream turbulence and pressure gradients on transition from laminar to turbulent conditions in boundary-layers has been investigated by Taylor [105] (1938), Schubauer and Skramstad [106] (1943), and Schlichting [107] (1962). Large fluctuations of

free-stream velocity due to turbulence, however, were not considered and their results do not seem to apply to flow through contractions.

In a recent paper by Miller and Fejer, [108] concerned with transition in Blasius-type boundary-layers, it was reported that the transition Reynolds number is influenced only by the amplitude of free-stream turbulent oscillations whereas the dimensionless transition length is controlled only by the frequency of free-stream turbulent oscillations. These factors demand investigation for various types of venturi meters.

6.8 General theoretical considerations

In support of the general theory, it must be stressed that most investigators have wrongly believed that a laminar boundary-layer at entrance to a meter is stabilised by decreasing pressure towards the throat and that, consequently, a laminar layer is triggered into transition only at entrance to the throat. Wind-tunnel experiments have confirmed that in fact steeply increasing pressures are developed at entrance to a conical section owing to reduction of curvature of the profile and that the intensity of this gradient can be sufficient to cause transition near the critical Reynolds number, before the end of the contracted section is reached. This

transition is not sudden but tends to 'develop' over a range of Reynolds numbers. From other investigations[3] it appears that boundary-layer transition takes place at Reynolds numbers between 10^5 and 10^6 - i.e. in the region appropriate to most measurements in practice.

This boundary-layer hypothesis also explains the fact that uncertainty in C_d- values, together with the retarded tendency to settle down to limiting values, is more pronounced in small than large throat meters. Large meters behave more rationally, possibly because of reduced influence of the transition spectrum.

In a strongly convergent nozzle, a turbulent boundary-layer, present from the outset, would be most unlikely. According to the above theory a laminar or a laminar-turbulent mixture could be expected in the boundary-layer for some distance from the start of the nozzle with completed transition probably confined to a particular zone, say at entrance to the throat or near the throat tapping (for conical meters). This would explain the flattening tendency of the C_d-characteristic at high Reynolds numbers.

7. DERIVATION OF AN EXPRESSION FOR CALCULATING C_d FROM EXPERIMENTAL RESULTS

Considering the original equation for a venturi

meter (equation 6.1), it is evident that, for a particular meter and fluid, this equation can be expressed as :

$$Q = C_d K \sqrt{\Delta_p}$$

or $$C_d = \frac{Q}{K\sqrt{\Delta_p}} \qquad \ldots\ldots\ldots\ldots\ldots\ldots \quad (6.12)$$

Thus, Q and Δ_p are measured experimentally whence C_d is calculated from equation (6.12).

The author submits that, at present, the accuracy with which Q is measured in a laboratory is higher than that with which Δ_p is determined. In the foregoing section it was shown that temperature, buoyancy, specific gravity and related corrections are necessary when measuring Q, to ensure accuracies of the order of 0.25 per cent in C_d. On the other hand, it is remarkable that corrections for static hole size, average pressure distribution and turbulence are neglected when Δ_p, the differential pressure, is measured. At this stage it is not known whether the above corrections would be masked by pressure fluctuations, but even if this were so, the average reading recorded should be corrected. The generally accepted form of the experimental characteristics could probably be influenced by these differential pressure corrections, especially over the lower Reynolds number

ranges. Accordingly, the following additional factors, which were dealt with earlier on, are considered :

7.1 Static pressure correction due to static hole size.

7.2 Average static pressure correction due to turbulence.

7.3 Correction of total energy equation due to turbulence.

In Chapter IV a static pressure correction due to the inherent static hole error was dealt with (Fig. 4.3). It will be assumed here that the corrected static pressure values for a venturi meter - depending on pipe diameter, static hole size and Reynolds number - can be written as P_{w1} and P_{w2} at entrance and meter throat respectively.

Due to turbulence, these corrected wall static pressures would be greater than the true average static pressure over a pipe cross-section. According to equation (4.10) in Chapter IV, this correction can be written as :

$$\frac{\overline{\Delta p}}{\overline{p}} = 1.26\, T_w$$

If the true average static pressures at entrance and in a venturi throat are therefore denoted by $\overline{P}_{s1}$ and $\overline{P}_{s2}$ then :

$$\overline{P}_{s1} = P_{w1} - 1.26\ T_{w1} \quad \ldots\ldots\ldots\ldots (6.13)$$

and $$\overline{P}_{s2} = P_{w2} - 1.26\ T_{w2} \quad \ldots\ldots\ldots\ldots (6.14)$$

Rewriting the general energy equation and allowing

for the factors mentioned above yields :

$$\bar{P}_{s1} + \tfrac{1}{2}\lambda_1\rho\overline{V_1^2} + \tfrac{1}{2}\rho(\overline{v_1'^2} + \overline{u_1'^2} + \overline{w_1'^2}) = \bar{P}_{s2} + \tfrac{1}{2}\lambda_2\rho\overline{V_2^2} + \tfrac{1}{2}\rho(\overline{v_2'^2} + \overline{u_2'^2} + \overline{w_2'^2}) + \frac{K_L\rho\overline{V_2^2}}{2} \quad \ldots\ldots\ldots (6.15)$$

$$\therefore \quad \beta(\bar{P}_{s1} - \bar{P}_{s2}) = \beta\bar{\Delta}_p = \tfrac{1}{2}\rho\overline{V_2^2}\,(\lambda_2 + K_L - \lambda_1 m'^2) + \tfrac{1}{2}\rho\,(\Sigma\overline{v_1'^2} - \Sigma\overline{v_2'^2})$$

$$\therefore \quad \overline{V_2^2} = \frac{2\beta\bar{\Delta}_p - \rho(\Sigma\overline{v_1'^2} - \Sigma\overline{v_2'^2})}{\rho\,(\lambda_2 + K_L - \lambda_1 m'^2)} \quad \ldots\ldots\ldots (6.16)$$

where $\bar{\Delta}_p = p_{w1} - p_{w2} + 1.26\,(T_{w1} - T_{w2})$ $\ldots\ldots (6.17)$

Now $Q = C_d A_2 V_2$, and substituting equation (6.16) for V_2 and neglecting K_L yields :

$$\therefore \quad Q = \frac{C_d A_2}{\sqrt{\lambda_2 - \lambda_1 m'^2}} \cdot \sqrt{\frac{2\beta\bar{\Delta}_p}{\rho} - (\Sigma\overline{v_1'^2} - \Sigma\overline{v_2'^2})} \quad \ldots\ldots\ldots (6.17)$$

$$\text{or} \quad C_d = \frac{\frac{Q}{A_2}\sqrt{\lambda_2 - \lambda_1 m'^2}}{\sqrt{\frac{2\beta\bar{\Delta}_p}{\rho} - (\Sigma\overline{v_1'^2} - \Sigma\overline{v_2'^2})}} \quad \ldots\ldots\ldots (6.18)$$

where $\overline{\Delta_p}$ represents the true corrected static pressure differential, the other symbols representing the original factor effects as defined.

As stressed in Chapter IV, the above corrections are possible and of value only if reliable experimental data on the r.m.s. values of turbulent velocity fluctuations in venturi meters are available whence C_d can be calculated from equation (6.18).

8, CONCLUSIONS

A detailed and comprehensive analysis was made of all the factors likely to influence the functioning of venturi meters. Theoretical expressions for calculating C_d were derived and the values thus calculated were compared with those of other investigators and with extensive experimental results from N.E.L. and Liège.

The final tests at N.E.L. and Liège show results which are in very close agreement with the author's theoretical values for Reynolds numbers 2×10^5 and higher, the maximum discrepancies being of the order of -0.4 per cent at the 'hump' and ranging from +0.03 to zero per cent for Reynolds numbers 4×10^5 and upwards.

In the laminar range, Hall's part of the proposed theoretical curve shows maximum deviations of approxi-

mately ± 0.3 per cent up to a Reynolds number of 1.5×10^5.

There seems to be theoretical verification of the hypothesis relating venturi meter characteristics to pipe friction curves. Laminar, transitional and turbulent zones in the characteristic curve have been suggested on experimental and theoretical grounds. Coefficients for the laminar and the turbulent ranges can be predicted very closely for conical-type meters. As in so many other fluid mechanics problems, the transition mechanism and transition Reynolds numbers still remain obstacles. The 'hump' which is also found in the pipe friction curves is, according to the theory advanced, due to the effect of separation and transition on the measured differential pressure over a given length of pipe. The author submits that if a correction for the effects of turbulence and static hole error were applied to differential pressure, the shape of the pipe friction curves over the transition zone would probably alter in the same way as does the characteristic curve of a venturi meter.

It is therefore suggested that in future experimental work on venturi meters, the measured differential pressure should be corrected for the effects of impact, turbulence structure, static hole error and average

static pressure in order to establish a more precise experimental characteristic. Transition Reynolds numbers and transition lengths should be investigated for various meters and for various turbulence structures in an attempt to correlate these factors with the newly established characteristics.

The theories advanced here will have to be extended to venturi meters having varying roughness values, area ratios, and geometrical shapes and receiving flows of various turbulence structures before the analysis and promising evidence submitted here can be considered conclusive. Numerous application of theoretical considerations will continue to meet with difficulties until venturi forms and designs, allowing better and more reliable flow rating coefficients are specified by International Codes.

In this respect, the following points are submitted for consideration :

6.1 A standard design should be established for universal use. Boundary-layer flow conditions, turbulence structure, area ratio and ease of manufacture should be considered in developing such a design.

6.2 Velocity profile at entrance to a meter should be controlled by rings or grooves in the approach pipe to

eliminate the effect of the approach pipe friction factor.

8.3 Internal meter roughness should be properly defined and standardised; as shown, this factor controls the major part of the meter characteristics.

8.4 The standard design should ensure that the boundary-layer is triggered at entrance to the meter to ensure that a uniformly accelerated turbulent boundary layer throughout is developed. Internal throat and divergent cone geometry should be such as to control this turbulent boundary-layer and ensure gradually increasing pressure thereby preventing the boundary-layer from reverting to laminar conditions.

The many hurdles blocking the path to the desired solution are evident. The author is of the opinion, however, that research methods and the general approach to the problem of flow through venturi meters should be brought in line with the analysis and suggestions contained in this Chapter. It is trusted that this will lead to reliable relationships for predicting discharge coefficients within specified limits of accuracy and thus render meter calibration superfluous.

APPENDIX I

NOTATION

a_b	Instrument constant.
A_1, A_2	Cross-sectional flow areas.
C_o, C_o', C_o''	Instrument coefficients.
C	Average sample concentration; mathematical constant.
C_d	Discharge coefficient of a venturi meter; drag coefficient for flow round a sphere.
C_f	Local coefficient of skin friction.
C_{h_1}, C_{h_2}	Instrument constants.
C_L	Coefficient of lift.
C_p	Pressure coefficient.
D	Diameter of sphere or pipe; current meter diameter.
B, B', B_o	Meter constants.
d	Diameter of frontal inlet to sphere.
d_p	Probe diameter.
d_s^p	Diameter of probe static hole.
d_s	Diameter of static pressure orifice.
$e = \frac{\epsilon_v}{D}$	The relative roughness.
F_o	Force due to external hydraulic resistance forces.

F_i	Internal friction force; impact force.
f	Coefficient of friction.
g	Function describing turbulent velocity distribution.
g'	Derivative of above function.
K	Pressure coefficient.
K_a, k_a, K_t	Instrument constants.
K_L	Losses through a venturi.
K_o	Instrument coefficient (spherical probe)
K'	Flow constant.
K_1, K_n...	Mathematical constants.
l_1, l_2	Equivalent friction lengths for flow through sphere.
m	Area ratio $= \frac{A_2}{A_1}$
m'_e	Altered area ratio due to laminar displacement thickness.
m'_t	Altered area ratio due to turbulent displacement thickness.
n	Number of current meter revolutions in unit time.
p_e	Static pressure at probe entrance.
p_o	Free stream static pressure.
p_f	Pressure caused by momentum change reaction force.
p_s	Static pressure.
p_t	Total pressure.

p_i	Impact pressure.
p_w	True static pressure at wall tapping.
q	Volume of injected dye.
R r	Pipe radii.
R_D	Pipe Reynolds number.
R_e	Reynolds number.
R_p	Reynolds number based on spherical probe diameter.
$R_d = R_e$	Reynolds number based on throat diameter.
s	Distance.
S	Theoretical length dimension associated with blade shape.
t	Time; temperature.
T	Torque developed.
T_b	Torque developed on blade.
T_h	Torque due to internal hydraulic resistance forces.
T_i	Torque due to F_i.
T_m	Torque due to internal mechanical resistance forces.
$\overline{U}$	True centre line velocity.
$\overline{U}_d$	True measured velocity due to displacement.
u_r	Friction velocity $= \sqrt{\frac{\tau_w}{\rho}}$
U_m	Mean conduit velocity.
$\overline{u'}$ $\overline{v'}$ $\overline{w'}$	Time average mean values of instantaneous turbulent velocity fluctuations in the x-, y- and z-directions.

$\overline{rv_1^2} = \overline{r'^2_1} + \overline{u'^2_1} + \overline{w'^2_1}$
$\overline{rv_2^2} = \overline{r'^2_2} + \overline{u'^2_2} + \overline{w'^2_2}$
Summation of mean squared turbulent velocity fluctuations.

$v, v_1, v_2 \ldots\ldots$
$v, v_1, v_2 \ldots\ldots$
Velocity of flow or velocity registered by a current meter

V_o Free stream velocity.

V_e Velocity at entrance to spherical probe.

$\overline{v}$ Time average point velocity.

V_r Relative velocity.

V_i Instantaneous resultant velocity.

$\overline{V}_m$, $\overline{V}_t$ Average velocities as determined from calibration tank and total pressure traverses respectively.

$\overline{v^2}$ Mean squared velocity.

x Diameter of tubular passage in sphere.

y Diameter of venturi orifice.

$\overline{y} = \frac{Y}{r}$, dimensionless position.

$f, X, F, f_1, f_2, f_3, f', f''$ Notations denoting a function.

α Angle of flow or angle of attack.

β Impact pressure coefficient.

A Instrument constant; the partial velocity of a current meter.

Δ_p Differential pressure; difference between true wall static pressure and that actually measured.

Δ'_p Turbulence error component in static pressure; differential pressure as measured.

$\overline{\Delta'_p}$ Average value of turbulence correction over a pipe cross-section.

δ_d Boundary-layer displacement thickness.

Δ_p^p Static pressure error due to probe static hole size.

Δ_p^t Probe static pressure error due to turbulence.

Φ_p Differential pressure relative to wake pressure
$\Phi_p = P_t - p(\text{wake})$

$n = \frac{Y}{X}$ spherical probe parameter.

ρ Mass density.

ν Kinematic viscosity.

ϕ_1 Angle of convergence.

ϕ_2 Angle of divergence.

ψ' Denotes function.

$\emptyset$ Diameter of central sting.

ω Angular speed of rotation.

ϑ, ϑ' Denotes function.

Ω_t Turbulence constant.

μ Viscocity.

T_w Wall shear stress.

Q Discharge.

ε Total energy.

λ_1)
λ_2) Kinetic energy coefficients.

λ_{s-1})
λ_{1-2}) Losses due to boundary resistance.

λ_s Losses due to resistance of central sting.

APPENDIX II

THEORETICAL ANALYSIS FOR SPHERICAL TOTAL PRESSURE PROBE

1. GENERAL EQUATION FOR TOTAL PRESSURE P_t

Referring to Fig. II.1 and applying the total energy equations between section (a) and section (2), the turbulence structure in the free-flow will be considered as approximately identical to that within the probe at section (1) and at exit at section (2). Provided the stream lines are deflected into the probe, this approximation should not prove unrealistic. Total pressure correction for turbulence is dealt with separately in Chapter III.

Thus, the effect of turbulence will be neglected here and hence the total energy equations can be written as :

$$p_o + \tfrac{1}{2}\rho v_o^2 = p_t = p_e + \tfrac{1}{2}\rho v_e^2 \quad \ldots\ldots\ldots\ldots \text{(II.1)}$$

and $$p_e + \tfrac{1}{2}\rho v_e^2 = p_1 + \tfrac{1}{2}\rho v_1^2 + \lambda_{e-1} + \lambda_s \quad \ldots\ldots\ldots \text{(II.2)}$$

where λ_{e-1} represents the losses due to boundary resistance between sections (e) and (1) and λ_s is the loss due to the blockage effect of the central sting.

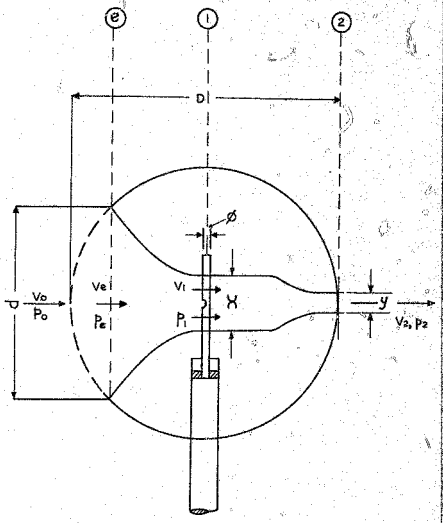

FIG. II.1

Between section (1) and (2) one can write :

$$p_1 + \tfrac{1}{2}\rho v_1^2 = p_2 + \tfrac{1}{2}\rho v_2^2 + \lambda_{1-2} \quad \text{.....(II.3)}$$

where λ_{1-2} is the pressure loss, due to boundary resistance, between sections (1) and (2).

The pressure at the 'exhaust' end of the probe can be expressed in terms of a pressure coefficient viz :

$$\frac{p_2 - p_0}{\tfrac{1}{2}\rho v_0^2} = C_p \quad \text{..... (II.4)}$$

where C_p is the base pressure coefficient. The total pressure p_t, which is registered by the probe at section (1), may be expressed as :

$$p_1 + \tfrac{1}{2}\rho v_1^2 = K_0 p_t \quad \text{..... (II.5)}$$

where K_0 is defined as the instrument coefficient. Equations (II.1), (II.2) and (II.3) yield :

$$p_0 + \tfrac{1}{2}\rho v_0^2 = p_t = p_2 + \tfrac{1}{2}\rho v_2^2 + \lambda_{e-1} + \lambda_{1-2} + \lambda_a \quad \text{..(II.6)}$$

Over the Reynolds number range tested the losses in equation (II.6) may be approximated by :

$$\lambda_{e-1} = K_1 v_1^2,$$

and

$$\lambda_{1-2} = K_2 v_2^2$$

The energy loss due to the blockage effect of the central sting may be calculated as follows :

The drag coefficient C_d, for a cylinder in the R_e range under consideration is approximately 1.2 (from standard graph).

$\therefore$ Drag on central sting = $C_d \frac{1}{2}\rho V_1^2 \phi x$

This drag force, expressed as a pressure operating over the central chamber, yields :

$$\lambda_s = \frac{1.2}{2} \cdot \frac{\rho V_1^2 \phi x}{Hx^2} = \frac{2.4 \rho V_1^2 \phi}{Hx} \quad \ldots\ldots\ldots (II.7)$$

Assuming that at the Reynolds numbers considered, and due to the retardation of flow at entrance, as postulated, the flow in the boundary-layer, inside the probe, takes place in the laminar or partly laminar range, an approximation for the friction factor, f, can be written as : $f = \frac{64}{R_e}$

Now $K_1 V_1^2 = \frac{\rho f \ell_1}{x} \cdot \frac{V_1^2}{2}$ where ℓ_1 is the equivalent friction length between section (e) and (1)

$$\therefore \quad K_1 V_1^2 = \frac{64\mu}{V_1 \rho x} \cdot \frac{\ell_1 V_1^2 \rho}{2x}$$

$$\therefore \quad K_1 = \frac{32\mu\ell_1}{x^2 V_1} \quad \ldots\ldots\ldots\ldots\ldots (II.8)$$

and similarly $K_2 = \frac{32\mu_2}{y^2 V_2}$ ..... (II.9)

Reverting now to equation (II.6), substitution for λ_{c-1}, λ_{1-2} and λ_s yields :

$$P_t = P_2 + \tfrac{1}{2}\rho V_c^2 + K_1 V_1^2 + K_2 V_2^2 + \frac{2.4\rho V_1^2 \phi}{\pi x} \quad \text{.....(II.10)}$$

The continuity equation between sections (1) and (2) yields : $V_2 = V_1 (\frac{x}{y})^2$.

Therefore rewriting in terms of V_1, equation (II.10) becomes :

$$P_t = P_2 + V_1^2 \left[\tfrac{1}{2}\rho (\tfrac{x}{y})^4 + K_1 + K_2 (\tfrac{x}{y})^4 + \frac{2.4\rho\phi}{\pi x} \right] \text{..(II.11)}$$

Equation (II.4) can be written as :

$$P_2 = C_p \tfrac{1}{2}\rho V_o^2 + P_o \quad \text{.....(II.12)}$$

Substituting equation (II.12) in equation (II.11) yields :

$$P_t = C_p \tfrac{1}{2}\rho V_o^2 + P_o + V_1^2 \left[\tfrac{1}{2}\rho (\tfrac{x}{y})^4 + K_1 + K_2 (\tfrac{x}{y})^4 + \frac{2.4\rho\phi}{\pi x} \right]$$

..... (II.13)

Substituting equation (II.1) in equation (II.13) yields :

$$P_t = C_p \tfrac{1}{2}\rho V_o^2 + P_e + \tfrac{1}{2}\rho V_e^2 - \tfrac{1}{2}\rho V_o^2 + V_1^2 \left[\tfrac{1}{2}\rho \left(\frac{x}{y}\right)^4 + K_1 + K_2 \left(\frac{x}{y}\right)^4 + \frac{2.b\rho\phi}{\pi x} \right]$$

Substituting equation (II.2) and (II.5) back in equation (II.14) yields :

$$P_t = \tfrac{1}{2}\rho V_o^2 (C_p - 1) + K_o P_t + K_1 V_1^2 + \frac{2.b\rho V_1^2 \phi}{\pi x} + V_1^2 \left[\tfrac{1}{2}\rho \left(\frac{x}{y}\right)^4 + K_1 + K_2 \left(\frac{x}{y}\right)^4 + \frac{2.b\rho\phi}{\pi x} \right]$$

$$\therefore \quad P_t (1 - K_o) = \tfrac{1}{2}\rho V_o^2 (C_p - 1) + V_1^2 \left[\tfrac{1}{2}\rho \left(\frac{x}{y}\right)^4 + 2K_1 + K_2 \left(\frac{x}{y}\right)^4 + \frac{2.b\rho\phi}{\pi x} \right] \qquad \text{.....(II.14)}$$

Now $V_e = K' V_o$, as defined originally,

and $V_1 = V_o \left(\frac{d}{x}\right)^2$ (from the continuity equation)

$\therefore \quad V_1 = K' V_o \left(\frac{d}{x}\right)^2$

Substituting this value for V_1, together with equations (II.8) and (II.9), in equation (II.14) yields :

$$P_t\ (1 - K_o) = \tfrac{1}{2}\rho V_o^2\ (C_p - 1) + (K')^2 V_o^2 \left(\frac{d}{x}\right)^4 \left[\tfrac{1}{2}\rho \left(\frac{x}{y}\right)^4 + \frac{64\mu x_1}{K' V_o d^2} + \frac{32\mu x_2}{K' V_o d^2}\left(\frac{x}{y}\right)^4 + \frac{4.8\rho g}{Hx}\right]$$

which on simplification yields :

$$P_t = V_o^2 \left\{ \frac{\rho}{2}\left[\frac{C_p - 1}{1 - K_o}\right] + \frac{(K')^2}{1 - K_o}\left[\frac{\rho}{2}\left(\frac{d}{y}\right)^4 + \frac{64\mu x_1}{K' V_o} \cdot \frac{d^2}{x^3} + \frac{32\mu x_2}{K' V_o} \cdot \frac{d^2}{y^4} + \frac{4.8\rho g}{H} \cdot \frac{d^4}{x^5}\right]\right\} \quad \ldots\ldots\ldots (II.15)$$

Equation (II.15) is the general theoretical expression for P_t as measured by a particular total-pressure probe in a velocity field flowing at velocity of V_o.

When comparing equations (II.15) and (3.4) in Chapter III, the functional relationship is clearly illustrated.

Equation (II.15) can be written in a simpler form as :

$$P_t = V_o^2 \left\{ C_1 + (K')^2\ C_2 \left[A_1 + \frac{A_2}{K'} + \frac{A_3}{K'} + A_4\right]\right\} \quad \ldots\ldots\ldots\ldots\ldots (II.16)$$

for a particular instrument where :

$$C_2 = \frac{1}{1 - K_o} ;$$

$$U_1 = \frac{\rho(\gamma_p - 1)}{2(1 - K_o)} ;$$

$$\Delta_1 = \frac{\pi d}{2y^4} ;$$

$$\Delta_2 = \frac{6h\mu_1 d^2}{V_o x^4} ; ;$$

$$\Delta_3 = \frac{32h\mu_2 d^2}{V_o y^4} , \text{ and}$$

$$\Delta_4 = \frac{4.8\rho\phi^4}{\pi x^5}$$

If, for a particular instrument, K_o, K' and C_p can be estimated the theoretical total pressure P_t would be given by equation (II.16).

2. THE DERIVATION OF AN EXPRESSION FOR V_2 IN ORDER TO ESTIMATE K' FROM V_o

According to the equation :

$$P_t = P_2 + \tfrac{1}{2}\rho V_2^2 + K_1 V_1^2 + K_2 V_2^2 + \frac{2.4\rho V_1^2 \phi}{\pi x} \quad \ldots\ldots(II.10)$$

Substituting $V_1 = V_2 \left(\frac{Y}{x}\right)^2$ and for K_1 and K_2 in equation (II.10) yields :

$$P_t = p_2 + \tfrac{1}{2}\rho V_2^2 + \frac{32\mu_1 V_2}{y^2} \cdot \frac{x^4}{x^4} + \frac{32\mu_2 V_2}{y^2}$$

$$+ \frac{2.4\rho V_2^2 g}{\pi x} \cdot \frac{x^4}{x^4} \quad \ldots\ldots\ldots\ldots \text{(II.17)}$$

According to equation (II.12)

$$P_2 = C_p \cdot \tfrac{1}{2}\rho V_o^2 + p_o$$

Substituting this equation in equation (II.17) and simplifying yields :

$$P_t - p_o = C_p \tfrac{1}{2}\rho V_o^2 + \tfrac{1}{2}\rho V_2^2 + \frac{32\mu_1 V_2 y^2}{x^4} + \frac{32\mu_2 V_2}{y^2}$$

$$+ \frac{2.4\rho V_2^2 g}{\pi} \cdot \frac{x^4}{x^5} \quad \ldots\ldots\ldots\ldots \text{(II.18)}$$

But $P_t - p_o = \tfrac{1}{2}\rho V_o^2$.

Therefore equation (II.18) becomes :

$$\tfrac{1}{2}\rho V_o^2 (1 - C_p) = \tfrac{1}{2}\rho V_2^2 + V_2 \left[\frac{32\mu_1 y^2}{x^4} + \frac{32\mu_2}{y^2}\right]$$

$$+ \frac{2.4\rho g y^4}{\pi x^5} \cdot V_2^2 \quad \ldots\ldots\ldots\ldots \text{(II.19)}$$

It is now clear that equation (II.19) can be

expressed as a quadratic in V_2, thus :

$$V_2^2\left[\frac{\rho}{2} + \frac{2.4\sigma g y^4}{Rx^5}\right] + V_2\left[\frac{32\mu_1 y^2}{x^4} + \frac{32\mu_2}{y^2}\right] + \tfrac{1}{2}\rho V_o^2 (C_p - 1) = 0$$

or $$AV_2^2 + BV_2 + C = 0 \quad \ldots\ldots\ldots\ldots\ldots\ldots \text{(II.20)}$$

where : $$A = \left[\frac{\rho}{2} + \frac{2.4\sigma g y^4}{Rx^5}\right] ;$$

$$B = \left[\frac{32\mu_1 y^2}{x^4} + \frac{32\mu_2}{y^2}\right], \text{ and}$$

$$C = \tfrac{1}{2}\rho V_o^2 (C_p - 1)$$

By applying equation (II.20) to a particular probe at a known free stream velocity, V_o, it is possible to calculate V_2 at an accepted C_p-value. From V_2, V_e can be determined, by the continuity equation, and hence K' may be estimated.

3. THE DERIVATION OF A RELATIONSHIP FOR K_o IN TERMS OF σ

Analysis of equation (II.16) shows that, for a particular probe, K_o can be expressed in terms of x and y, and that it should therefore, be possible to calcu-

late K_o, uniquely, for a particular instrument, in terms of σ, if V_o and C_p are known.

The general equation (II.16) may be written as :

$$\frac{P_t}{\frac{\rho}{2}V_o^2} = \frac{\rho}{2}\left[\frac{C_p - 1}{1 - K_d}\right] + \frac{(K')^2}{1 - K_o}\left\{\frac{\rho}{2}\left(\frac{d}{y}\right)^4 + \frac{64\mu L_1}{K'V_o}\cdot\frac{d^2}{x^4} + \frac{32\mu L_2}{K'V_o}\cdot\frac{d^2}{y^4} + \frac{4.8\rho g}{\Pi}\cdot\frac{d^4}{x^3}\right\}$$

$$\therefore \frac{P_t}{\frac{\rho}{2}V_o^2}(1 - K_o) = \frac{\rho}{2}(C_p - 1) + (K')^2\left\{\frac{\rho}{2}\left(\frac{d}{y}\right)^4 + \frac{64\mu L_1}{K'V_o}\cdot\frac{d^2}{x^4} + \frac{32\mu L_2}{K'V_o}\cdot\frac{d^2}{y^4} + \frac{4.8\rho g}{\Pi}\cdot\frac{d^4}{x^3}\right\}$$

Hence :

$$K_o = 1 - \frac{V_o^2}{P_t}\left\{A_1 + (K')^2\left[\frac{G_1}{y^4} + \frac{G_2}{K'x^4} + \frac{G_3}{K'y^4} + \frac{G_4}{x^3}\right]\right\}$$

$$\text{or } K_o = 1 - \frac{V_o^2}{P_t}\left\{A_1 + (K')^2\left[\frac{G_1}{x^4\sigma^4} + \frac{G_2\sigma^4}{K'y^4} + \frac{G_3}{K'\sigma^4x^4} + \frac{G_4\sigma^5}{y^5}\right]\right\} \quad \ldots\ldots\ldots\ldots(II.21)$$

where : $A_1 = \frac{\rho}{2}(C_p - 1)$;

$G_1 = \frac{\rho d^4}{2}$;

$G_2 = \frac{64\mu z_1 d^2}{V_o}$;

$G_3 = \frac{32\mu z_2 d^2}{V_o}$, and

$G_4 = \frac{4.8\rho d^4}{\Pi}$

Therefore, by equation (II.21), K_c can be calculated for a probe of known dimensions in terms of d, its corresponding K'-values, and for $C_p = -0.4$, and -0.2, at any free-stream velocity V_o. Sample calculations are shown in Appendix III.

APPENDIX III

SAMPLE CALCULATIONS AND TABULATED RESULTS FOR SPHERICAL TOTAL PRESSURE PROBE

In this Appendix the theoretical equations were evaluated by substituting data from probes on actual test.

1. GRAPH NO. 1 AND NO. 2 IN FIGURE 3.22

K' was calculated for different values of σ from equation :

$$AV_2^2 + BV_2 + C = 0 \quad \text{.....(II.20)}$$

or $$V_2^2 \frac{\rho}{2} + \frac{2\mu\sigma y^4}{Hx^5} + V_2 \frac{32\mu x_2}{y^2} + \frac{32\mu x_2 y^2}{x^4}$$

$$+ \tfrac{1}{2}\rho V_o^2 (C_p - 1) = 0$$

and from the relationships :

$$V_e d^2 = V_2 y^2 \quad \text{and}$$

$$V_e = K' V_o \quad \text{.....(3.7)}$$

The following values were substituted :

d = 0.02775 ft

σ = 0.336

ρ = 0.00234 slugs per ft^3

$\emptyset$ = 0.00458 ft

y = 0.005833 ft

x = 0.0173 ft

μ = 3.75×10^{-7} slugs per ft sec

t_2 = 0.0149 ft

t_1 = 0.01008 ft

c_p = -0.40

v_o = 217.357 ft per sec

The results are given in Tables III.1 and III.2

TABLE III.1

Graph No. (1)

c_p = -0.4	
σ	K'
0.336	0.0910
0.486	0.0907
0.765	0.2582

TABLE XII.2

Graph No. (2)

C_p = -0.2	
σ	K'
0.260	0.0251
0.326	0.0478
0.446	0.0840
0.765	0.2286

2. GRAPH NO. 3 IN FIGURE 3.22

Values for the venting orifice, y, were calculated for different assumed K'-values yielding theoretical σ-values for corresponding K'-values according to the equation :

$$P_t = V_o^2 \left\{ \frac{\rho}{2} \left[\frac{C_p - 1}{1 - K_o} \right] + \frac{(K')^2}{1 - K_o} \left[\frac{\rho}{2} \left(\frac{a}{y} \right)^4 + \frac{64\mu^2 a^2}{K' V_o y^4} + \frac{32\mu^2 \rho a^2}{K' V_o y^4} + \frac{4.8 \rho V a^4}{R y^5} \right] \right\} \quad \text{..... (II.15)}$$

The following values were substituted :

d = 0.019 ft

x = 0.012 ft

ℓ_1 = 0.01008 ft

ℓ_2 = 0.01496 ft

K' = 0.01

K_o = 0.991

C_p = -0.4

Values for the remaining symbols are identical to those used in Section 1.

The diameters of the probes tested were 0.3 inch, 0.5 inch and 0.344 inch, giving an average value of 0.38 inch. In view of the internal geometry of the different probes, the values of ℓ_1 and ℓ_2 were chosen such that $\ell_1 + \ell_2$ = 0.3 inch (0.025 ft) throughout.

The results are given in Table III.3

Tab. III.3

Graph No. 3

y (CALCULATED)	
d	K'
0.1440	0.010
0.3114	0.50
0.4419	0.15
0.6460	0.20

3. GRAPH NO. 4 AND NO. 5 IN FIG. 3.23

Values for K_o were calculated for different σ-values, using C_p-values of -0.2 and -0.4 and probe dimensions, in equation :

$$K_o = 1 - \frac{V^2}{P_t}\left\{ A_1 + (K')^2 \left[\frac{G_1}{x^4 \sigma^4} + \frac{G_2 \sigma^4}{K' y^4} + \frac{G_3}{K' \sigma^4 x^4} + \frac{G_4 \sigma^5}{y^5} \right] \right\} \quad \ldots\ldots\ldots\ldots\ldots\ldots\ldots\ldots\ldots\ldots \text{(II.21)}$$

Expressions for A_1 and G_1, G_2, G_3 and G_4 are give in Appendix II.

The following values were substituted :

d = 0.2775 ft

x = 0.01733 ft

y = 0.01325 ft

C_p = -0.4

σ = 0.765

K' = 0.25281

t_1 = 0.01008 ft

t_2 = 0.01496 ft

Values for the remaining symbols are identical to those used in the previous calculations.

The results are given in Tables III.4 and III.5.

TABLE III.4

Graph No. 4

$C_p = -0.2$	
σ	K_o
0.26	0.9997
0.336	0.9997
0.446	0.9996
0.765	0.9977

TABLE III.5

Graph No. 5

$C_p = -0.4$	
σ	K_o
0.336	1.0006
0.446	0.9991
0.765	0.9956

	CALIBRATION USED							
	N.P.L.$_I$				N.P.L.$_{II}$			
TEST	Q_m	Q_t	ΔQ	ϵ	Q_m	Q_p	ΔQ	ϵ
1.1-1.4	19.523	19.550	+0.027	+0.138	19.634	19.550	+0.084	+0.4
2.1-2.2	17.484	17.500	+0.016	+0.092	17.568	17.500	+0.068	+0.4
3.1-3.2	16.285	16.310	+0.025	+0.153	16.362	16.310	+0.052	+0.3
4.1-4.2	14.01	14.01	0.0	0.0	14.064	14.010	+0.054	+0.4
5.1-5.2	6.812	6.680	-0.132	-1.98	6.808	6.680	+0.128	+1.9
6.1-6.2	4.15	4.02	-0.130	-3.24	4.125	4.020	+0.105	+2.6
7.1-7.2	10.550	10.508	-0.042	-0.40	10.582	10.508	+0.074	+0.7
8.1-8.2	17.254	17.260	+0.006	+0.035	17.342	17.260	+0.082	+0.5
9.1-9.2	18.96	19.10	+0.04	+0.22	18.147	18.100	+0.047	+0.3

PERCENTAGE DEVIATIONS ϵ OF FLOW RATES DETERMINED BY CURRENT METERS IN 20-INCH CALIBRATION [illegible] FROM WEIGH-TANK RESULTS

APPENDIX V

THE DETERMINATION OF λ_1, λ_2, K_1, β AND THE BOUNDARY-LAYER EFFECT

1. THE KINETIC ENERGY COEFFICIENTS λ_1 AND λ_2.

Non-uniformity of velocity distribution outside the boundary-layer in pipe flow necessitates evaluation of λ_1 and λ_2.

Referring to Fig. V.1, the kinetic energy of an elementary ring at radius r_1 at section (1) and r_2 at section (2), is expressed as a fraction of the total kinetic energy in terms of the average velocity over the particular cross-section considered. Integrating over the cross-sections yields λ_1 and λ_2. Considering section (1) : At radius r_1, the mass flowing = $2\pi r_1 dr_1 v_1 \rho$ = m. The velocity of flow for this ring is = v_1.

$$\therefore \quad \tfrac{1}{2}mv_1^2 = \rho\pi r_1 v_1^3 dr_1$$

If the average velocity at section (1) is given by V_1, the total kinetic energy is given by :

$$\tfrac{1}{2}MV_1^2 \,,$$

where : $M = \pi R_1^2 V_1 \rho$

VELOCITY DISTRIBUTION AT SECTION ①

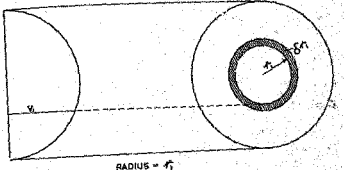

RADIUS = r_1
AV. VELOCITY = V_1

VELOCITY DISTRIBUTION AT SECTION ②

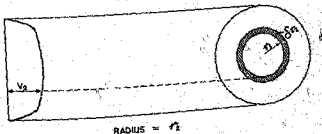

RADIUS = r_2
AV. VELOCITY = V_2

FIG. V-1

$\therefore$ Kinetic energy = $\frac{1}{2}\pi R_1^2 V_1^3 \rho$,

and according to the definition, $\delta\lambda_1$ can be written as :

$$\delta\lambda_1 = \frac{2\rho\pi r_1 V_1^3 \delta r_1}{\rho\pi R_1^2 V_1^3}$$

$$\therefore \delta\lambda_1 = 2\left(\frac{V_1}{V_1}\right)^3 \cdot \frac{r_1}{R_1^2} \cdot \delta r_1 \quad \ldots\ldots\ldots(V.1)$$

In the limit equation (V.1) can be written as :

$$d\lambda_1 = 2\left(\frac{V_1}{V_1}\right)^3 \cdot \left(\frac{r_1}{R_1}\right) \cdot \frac{dr_1}{R_1} \quad \ldots\ldots\ldots (V.2)$$

Transforming equation (V.2) by putting $\frac{r_1}{R_1} = u$ yields :

$$du = d\left(\frac{r_1}{R_1}\right) = \frac{dr_1}{R_1}$$

Substituting for $\frac{dr_1}{R_1}$ in equation (V.2) and integrating yields :

$$\int d\lambda_1 = \lambda_1 = 2\int_0^1 \left(\frac{V_1}{V_1}\right)^3 \cdot \left(\frac{r_1}{R_1}\right) \cdot d\left(\frac{r_1}{R_1}\right) \quad \ldots(V.3)$$

Similarly : $\lambda_2 = 2\int_0^1 \left(\frac{V_2}{V_2}\right)^3 \cdot \left(\frac{r_2}{R_2}\right) \cdot d\left(\frac{r_2}{R_2}\right) \quad \ldots(V.4)$

It is clear from equations (V.3) and (V.4) that the velocity distribution at a particular section is accounted for in the expressions for λ_1 and λ_2 in the light of the Prandtl-Rakhmeteff equation which defines

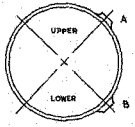

DIAGRAM OF VELOCITY PROBE POSITIONS

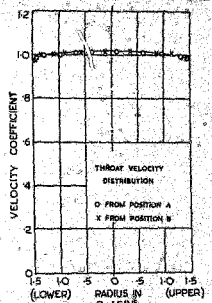

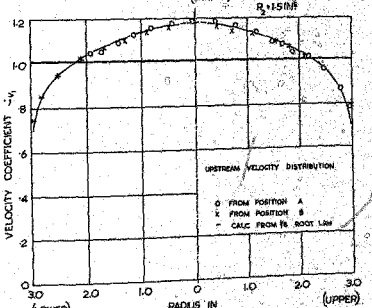

FIG. V 2 VELOCITY DISTRIBUTIONS THROUGH THE 6 IN. NEL-VENTURIMETER.

the velocity distribution in a circular pipe for turbulent flow, and which can be approximated by :

$$\frac{V}{\bar{V}} = 1 + 2.5\sqrt{\frac{f}{8}}\left[\frac{3}{2} + \log\left(1 - \frac{r}{R}\right)\right] \quad \ldots\ldots (V.5)$$

where f is the pipe friction coefficient given by :

$$f = \frac{2gH_d}{LV^2}$$

It must be stressed here that equation (V.5) does not satisfy conditions near a pipe wall when $\frac{r}{R}$ tends to unity. However, the errors involved are small, and can be neglected in practice.

Substituting equation (V.5) in equation (V.3) yields :

$$\lambda_1 = 1 + 2.93f - 1.55f^{3/2} \quad \ldots\ldots\ldots\ldots (V.6)$$

(87)

Thus λ_1 and λ_2 can be calculated when the coefficient of friction, f, at a particular Reynolds number is known. Values for λ_1 and λ_2 can also be determined from velocity traverses immediately upstream, and at the throat of a venturi. At N.E.L. (99) such traverses were carried out on a 6-inch venturi meter over two diameters. The results were plotted as velocity coefficients against pipe radius (Fig. V.2). From these plots equation (V.3) and (V.4) were evaluated, yielding values of 1.047 and 1.001 for λ_1 and λ_2 respectively, at a R_D of approximately 2×10^5. These values checked with those determined

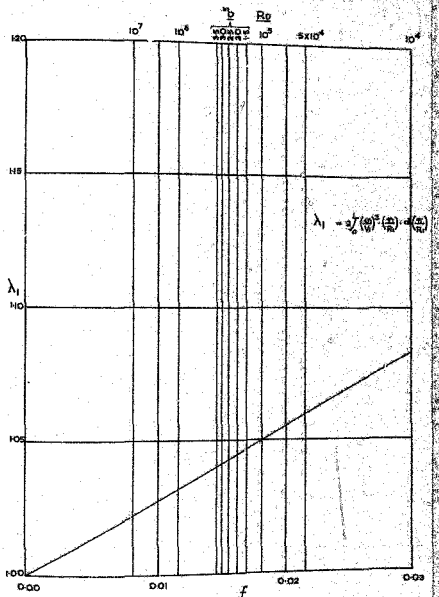

FIG. V·3 FACTOR λ_1

by direct integration. For normal Reynolds number ranges and roughness values in practice, f, varies between 0.01 and 0.04 giving corresponding λ_1 values ranging from 1.03 to 1.11, while λ_2 is usually taken as 1.00 (as the above experimental and calculated values indicate). Ferron [100] determined λ_2 as 1.000 while Coleman, [101] Furáy [102] and Foster [103] determined approximate values of 0.996, 1.002 and 1.017 for λ_2 respectively. In the light of the above evidence, a value of 1.00 for λ_2 seems reasonable provided $m \leq 0.3$.

Figure V.3 shows calculated values for λ_1, for different values of f, at various Reynolds numbers by applying equation (V.6). From the graph it is clear that $\lambda_1 = 1.044$ for a pipe Reynolds number of 2×10^5.

2. THE DETERMINATION OF K_L

To calculate the nozzle-losses in a venturi meter remains an obstacle due to the converging, throat and diverging flow conditions. Several attempts have been made to derive a workable expression for this parameter without any practical success.

The author attempted to evaluate K_L by applying the principle from which the impact pressure factor was derived. The resulting K_L-values agreed exactly with those obtained from the Hutton formula for a classical

venturi meter ($m = 0.25$), but were not in agreement for meters of larger area ratio.

Hutton [87] suggested a method by which nozzle-losses are referred to losses in an equivalent pipe length having the same diameter as the venturi throat, and arrived at the relationship :

$$K_L = f \frac{\ell}{d} \qquad \text{..... (V.7)}$$

where

ℓ is equivalent to a length of pipe of diameter d over which the head lost is identical to the head lost over the venturi meter, and

d = diameter of venturi throat.

Hutton showed that K_L can be predicted fairly accurately when $\frac{\ell}{d}$ is taken as approximately 2. He accordingly estimated C_d-values to an accuracy of $\pm$ 0.1 per cent when comparing calculated to measured values. This result is however not conclusive owing to the fact that the errors inherent in measuring the head lost over the meter are caused by the very factors one is attempting to eliminate; impact, for instance is neglected. It should be pointed out that the angle of convergence, which decidedly affects these losses, is functionally related to $\frac{\ell}{d}$ in the above relationship, and hence a fixed value

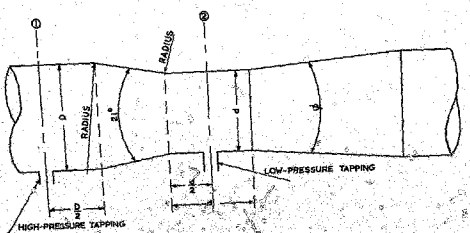

FIG. V4 HERSCHEL OR CONICAL VENTURI TUBE.

of $\frac{L}{d} = 2$ would be subject to error when considering different meters. However, this value of $\frac{L}{d}$ is substantiated by experimental backing, for the meter under consideration, and the author therefore accepts Hutton's expression.

Hence, $K_L \propto 2f$ ..... (V.8)

3. THE DETERMINATION OF δ

Engel and Davies [92] attempted to formulate this correction factor in 1938 while Engel [93] again referred to it briefly in 1953. Because the author does not agree with their theoretical approach, a different method is postulated : Streamlines are considered as being squeezed together at entrance to a venturi meter. This causes 'impact' and a pressure rise at the inlet pressure tapping. This squeezed flow through the venturi also precipitates an overall energy loss and hence a differential pressure higher than the true value is registered.

The mathematical method employed is as follows :

The rate of change of momentum between sections (1) and (2) (Fig. V.4) represents the force and hence the pressure which causes flow through the venturi. This is not what is sought; the rate of change of axial

momentum which gives rise to the 'impact pressure', is required.

The author therefore established relationships for momentum at sections (1) and (2). The momentum at section (2) was then transformed mathematically to section (1) to determine what the momentum at section (2) would have been at section (1) before the influence of stream tube bending, and associated energy losses. The expression representing the difference between the momentum at section (1) and the transformed momentum equation would thus define the reaction force which causes the impact pressure. Momentum correction factors, due to non-uniformity of the velocity distribution outside the boundary-layer, are also considered.

Referring to Fig. V.1 we have :

Average velocity over ring at radius $r_1 = v_1$

$\therefore$ ring momentum $= mv_1$ .....(m = mass)

and $m = 2\pi r_1 \delta r_1 \rho v_1$

$\therefore$ ring momentum $= 2\pi r_1 \delta r_1 \rho v_1^2$ ..... (V.9)

The section momentum $= \pi R_2^2 \rho v_2^2$ ..... (V.10)

If now K_{m1} and K_{m2} are defined as the momentum coefficients, equations (V.9) and (V.10) yield :

$$\delta K_{m1} = \frac{2\pi r_1 dr_1 \rho v_1^2}{\pi R_1^2 \rho V_1^2}$$

$$= 2\left(\frac{v_1}{V_1}\right)^2 \cdot \left(\frac{r_1}{R_1}\right) \cdot d\left(\frac{r_1}{R_1}\right)$$

$$\therefore K_{m1} = \int \delta K_{m1} = 2 \int_0^1 \left(\frac{v_1}{V_1}\right)^2 \cdot \left(\frac{r_1}{R_1}\right) \cdot d\left(\frac{r_1}{R_1}\right) \quad \ldots (V.11)$$

and similarly :

$$K_{m2} = 2 \int_0^1 \left(\frac{v_2}{V_2}\right)^2 \cdot \left(\frac{r_2}{R_2}\right) \cdot d\left(\frac{r_2}{R_2}\right) \quad \ldots\ldots\ldots (V.12)$$

One can now write the momentum at sections (1) and (2) in terms of the above momentum coefficients and the average velocities at the two sections viz :

Momentum at section (1) :

$$= K_{m1} M_1 V_1$$

$$= 2\pi R_1^2 \rho V_1^2 \int_0^1 \left(\frac{v_1}{V_1}\right)^2 \cdot \left(\frac{r_1}{R_1}\right) \cdot d\left(\frac{r_1}{R_1}\right) \quad \ldots\ldots\ldots (V.13)$$

and,

Momentum at section (2) :

$$= K_{m2} M_2 V_2$$

$$= 2\pi R_2^2 \rho V_2^2 \int_0^1 \left(\frac{v_2}{V_2}\right)^2 \cdot \left(\frac{r_2}{R_2}\right) \cdot d\left(\frac{r_2}{R_2}\right) \quad \ldots\ldots\ldots (V.14)$$

Equation (V.14) now represents the true momentum at section (2). Transforming this equation to section (1) yields :

$$\frac{v}{V} = F\left(\frac{r}{R}\right) \qquad \text{..... (V.15)}$$

Equation (V.15) represents the well-known Prandtl-Backmeteff equation, which defines the velocity distribution in a circular pipe for turbulent flow and for different values of the coefficient of pipe friction f. Mathematically, r_2 can written as r_1 and therefore v_2 as v_1,

also :

$$\frac{\pi R_2^2}{\pi R_1^2} = \frac{A_2}{A_1} = m = \left(\frac{R_2}{R_1}\right)^2$$

$$\therefore \quad R_2 = \sqrt{m}\, R_1 \qquad \text{..... (V.16)}$$

The continuity equation yields :

$$A_1 V_1 = A_2 V_2$$

$$\therefore \quad V_2 = \frac{V_1}{m} \qquad \text{..... (V.17)}$$

Substituting equations (V.16) and (V.17) in (V.14) yields :

Transformed momentum from section (2) to (1)

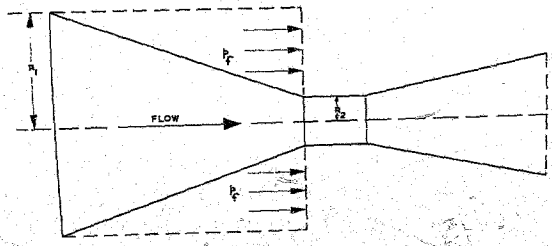

FIG. V.5 DETERMINATION OF IMPACT PRESSURE

$$= 2\pi R_1^2 \rho V_1^2 \left[\int_0^{\sqrt{n}} f\left(\frac{v_1}{V_1}\right)^2 \cdot \left(\frac{r_1}{R_1}\right) \cdot d\left(\frac{r_1}{R_1}\right) \right] \quad \ldots\ldots\ldots\ldots (V.18)$$

The difference between the momentum at section (1) (Equation V.13) and the transformed momentum equation (Equation V.18) represents the 'impact force'.

i.e. $$F_i = 2\pi R_1^2 \rho V_1^2 \left[\int_0^1 f\left(\frac{v_1}{V_1}\right)^2 \cdot \left(\frac{r_1}{R_1}\right) \cdot d\left(\frac{r_1}{R_1}\right) \right]$$

$$- 2\pi R_1^2 \rho V_1^2 \left[\int_0^{\sqrt{n}} f\left(\frac{v_1}{V_1}\right)^2 \cdot \left(\frac{r_1}{R_1}\right) \cdot d\left(\frac{r_1}{R_1}\right) \right] \text{ where}$$

F_i = force due to impact.

$$\text{or } F_i = 2\pi R_1^2 \rho V_1^2 \left[\int_{\sqrt{n}}^1 f\left(\frac{v_1}{V_1}\right)^2 \cdot \left(\frac{r_1}{R_1}\right) \cdot d\left(\frac{r_1}{R_1}\right) \right] \quad \ldots\ldots\ldots (V.19)$$

Referring to Fig. V.5, let p_f represent the pressure on a converging cone due to contraction of the stream lines. Then,

$$p_f \pi (R_1^2 - R_2^2) = 2\pi R_1^2 \rho V_1^2 \left[\int_{\sqrt{n}}^1 f\left(\frac{v_1}{V_1}\right)^2 \cdot \left(\frac{r_1}{R_1}\right) \cdot d\left(\frac{r_1}{R_1}\right) \right]$$

$$\therefore \quad p_f = \frac{1}{1-n} 2\rho V_1^2 \left[\int_{\sqrt{n}}^1 f\left(\frac{v_1}{V_1}\right)^2 \cdot \left(\frac{r_1}{R_1}\right) \cdot d\left(\frac{r_1}{R_1}\right) \right] \quad \ldots\ldots (V.20)$$

If p_i = impact pressure, this pressure can be written

as :

$P_i = K P_f$, defining P_i as : $P_i = \frac{\beta' \rho V_1^2}{2}$ and K, a constant depending on the geometry of the meter.

$$\therefore P_i = \frac{K}{1-m} \cdot 2\rho V_1^2 \int_{\sqrt{m}}^{1} \left(\frac{V_1}{V_1}\right)^2 \cdot \left(\frac{r_1}{R_1}\right) \cdot d\left(\frac{r_1}{R_1}\right)$$

$$= \frac{\beta' \rho V_1^2}{2}$$

$$\therefore \beta' = \frac{4K}{1-m} \left[\int_{\sqrt{m}}^{1} \left(\frac{V_1}{V_1}\right)^2 \cdot \left(\frac{r_1}{R_1}\right) \cdot d\left(\frac{r_1}{R_1}\right) \right] \quad \ldots\ldots (V.21)$$

where β' represents the fraction of the kinetic energy at inlet which is transformed to impact pressure.

Now an expression for β, the impact pressure correction factor, can be determined by expressing the impact pressure as a percentage of the measured differential pressure, thus :

Differential pressure measured $= P_1 + P_i - P_2 = \Delta p'$ and,

true differential pressure $= P_1 - P_2 = \Delta p$

The ratio $\frac{P_i}{P_1 + P_i - P_2}$ can therefore be

written as $$\frac{\frac{1}{2}\beta' \rho V_1^2}{p_1 + \beta' \rho V_1^2 - p_2} = \frac{\Delta'_p - \Delta_p}{\Delta'_p} \quad \ldots(V.22)$$

Also

$$p_1 + \frac{\rho V_1^2}{2} = p_2 + \frac{\rho V_2^2}{2} + K_L \frac{\rho V_2^2}{2}$$

$$\therefore \quad p_1 - p_2 = \Delta_p = \frac{\rho V_1^2}{2}\left[\frac{K_L + 1}{m^2} - 1\right] \quad \ldots(V.23)$$

Substituting for $p_1 - p_2$ in equation (V.22) yields :

$$\frac{\Delta'_p - \Delta_p}{\Delta'_p} = \frac{\beta' m^2}{K_L + 1 - m^2(1 - \beta')} \quad \ldots(V.24)$$

From equation (V.24) it follows that :

$$\Delta_p = \Delta'_p\left[1 - \frac{\beta' m^2}{K_L + 1 - m^2(1 - \beta')}\right]$$

or $\Delta_p = \beta \Delta'_p$ where β is defined as :

$$\beta = 1 - \frac{\beta' m^2}{K_L + 1 - m^2(1 - \beta')} \quad \ldots(V.25)$$

At this stage only a value β' remains to be determined in order to calculate β.

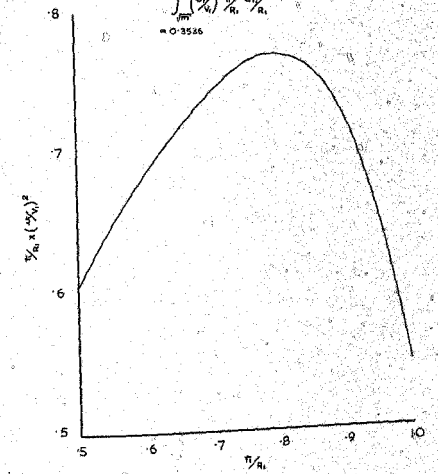

FIG. V.6 EXAMPLE OF THE DETERMINATION OF $\int_{\eta_{R_1}}^{1}$ FROM THE VELOCITY PROFILE.

3.1 Evaluation of $\int_{\sqrt{m}}^{1} f(\frac{y}{y_1}) \cdot (\frac{v}{v_1})^2 \cdot (\frac{r_1}{R_1}) \cdot d(\frac{r_1}{R_1})$ from velocity profiles

The experimental data in Fig. V.2 was used to plot $(\frac{v}{v_1})^2 \cdot (\frac{r_1}{R_1})$ against $(\frac{r_1}{R_1})$ as shown in Fig. V.6. From this the above integral was evaluated as 0.3516.

In verification of the mathematical relationships, the values of K_{m1} and K_{m2} were also determined, yielding :

$$K_{m1} = 1.02, \text{ and}$$

$$K_{m2} = 1.00$$

These values are to be expected due to the exceptionally good velocity profiles in question.

3.2 Evaluation of $\int_{\sqrt{m}}^{1} f(\frac{v}{v_1})^2 \cdot (\frac{r_1}{R_1}) \cdot d(\frac{r_1}{R_1})$ by direct integration

The above integral can be expressed as :

$$\int_{\sqrt{m}}^{1} F(\frac{r}{R})^2 \cdot (\frac{r}{R}) \cdot d(\frac{r}{R}) \quad \text{where } F(\frac{r}{R})$$

is the Prandtl-Bakhmeteff equation viz :

$$\frac{v}{V} = F(\frac{r}{R}) = \frac{1}{K}\sqrt{\frac{f}{8}} \left[\frac{3}{2} + K\sqrt{\frac{8}{f}} + \text{Log}\,(1 - \frac{r}{R})\right]_{K=0.4} \quad \ldots\ldots\ldots (V.26)$$

Substituting equation (V.26) yields :

$$\int_{\sqrt{m}}^{1} \left(\frac{r_1}{v_1}\right)^2 \cdot \left(\frac{r_1}{R_1}\right) \cdot d\left(\frac{r_1}{R_1}\right) = \int_{\sqrt{m}}^{1} \left\{\frac{1}{K}\sqrt{\frac{r}{\delta}}\left[\frac{3}{2} + K\sqrt{\frac{\delta}{r}} + b_m\left(1 - \frac{r}{R}\right)\right]^2\right\}_{K=0.4} \times \frac{r}{R} \cdot d\left(\frac{r}{R}\right) \qquad (V.27)$$

The right hand side of equation (V.27) can be written as :

$$a^2 \int_0^{1-\sqrt{m}} (b + \log z)^2 \cdot (1 - z) \cdot dz \qquad \ldots\ldots\ldots\ldots (V.28)$$

where $a = \frac{1}{K}\sqrt{\frac{r}{\delta}}$,

$b = \left(K\sqrt{\frac{\delta}{r}} + \frac{3}{2}\right)$, and

$z = \left(1 - \frac{r}{R}\right)$

To facilitate handling, equation (V.28) can be split up into :

$$a^2 \int_0^{1-\sqrt{m}} b^2 + 2b \log z + (\log z)^2 \, dz$$

$$- a^2 \int_0^{1-\sqrt{m}} zb^2 + 2bz \log z + z(\log z)^2 \, dz \qquad \ldots\ldots\ldots (V.29)$$

Integrating equation (V.29) by parts and substituting $K = 0.4$, $b_m = 0.25$ and $r = 0.02$ yields :

$$\int_{\sqrt{m}}^{1} \left(\frac{v_1}{V_1}\right)^2 \cdot \left(\frac{r_1}{R_1}\right) \cdot d\left(\frac{r_1}{R_1}\right) = 0.3847$$

This value is of the same order as that determined for a 6 inch nozzle-type N.E.L. venturi meter from actual velocity profiles viz : 0.3536, the discrepancy being approximately 7.8%. The value of 0.3847 would therefore be accepted for f = 0.02. Other values of this integral for different coefficients of friction and m = 0.25, are as follows :

f	$\int_{\sqrt{m}}^{1} \ldots$
0.011	0.3809
0.02	0.3847
0.03	0.3887

3.3 The determination of δ

In the foregoing theory, an expression for δ' was derived viz :

$$\delta' = \frac{4K}{1-m}\left[\int_{\sqrt{m}}^{1} \left(\frac{v_1}{V_1}\right)^2 \cdot \left(\frac{r_1}{R_1}\right) \cdot d\left(\frac{r_1}{R_1}\right)\right] \quad \ldots\ldots\ldots\ldots (V.21)$$

The above table shows how the integral in square brackets vary with coefficient of friction for constant area ratio. The author submits that K - which was

defined as that fraction of the pressure on a converging cone which is transformed into so-called impact pressure - would be a constant for a particular type of instrument depending on the contraction and internal geometry only. Therefore, K would be considered as a constant for say a nozzle-type venturi meter at a particular area ratio, and β' would be dependent on f and m only.

Now equation (V.24) defines β' as :

$$\frac{\text{impact pressure } p_i}{\text{measured differential pressure } \Delta p} = \frac{\beta' m^2}{K_L + 1 - m^2(1 - \beta')} \quad \ldots\ldots\ldots\ldots\ldots\ldots \text{(V.24)}$$

and it follows that if the left hand side of equation (V.24) can be measured experimentally, β' could be calculated for a particular instrument and given f and m values, whence K could be determined from equation (V.21). If, as submitted above, K is considered as a constant for the particular instrument, different values for β', depending on different f and m values, could be calculated yielding corresponding β values in terms of equation (V.25) viz :

$$\beta = 1 - \frac{\beta' m^2}{K_L + 1 - m^2(1 - \beta')} \quad \ldots\text{(V.25)}$$

Witte, Engr[illegible]anach (93) did measure

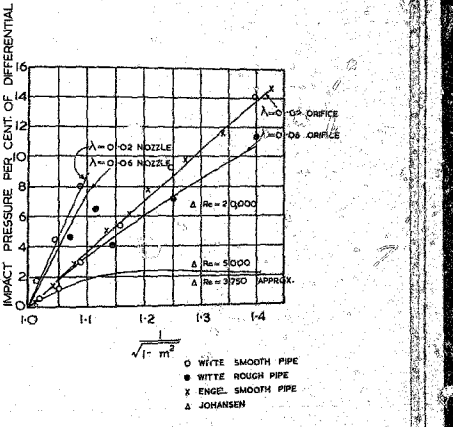

FIG. V-7 IMPACT PRESSURE

this impact pressure for nozzle and orifice-type instruments and expressed it as a percentage of the measured differential pressure for different values of f and m as shown in Fig. V.7. From these graphs the impact pressure factors are 0.032 and 0.017 at an area ratio of 0.25 and f = 0.02 for nozzle- and orifice-type venturi meters respectively.

Applying equations (V.21) and (V.24) as outlined above gives the following values for K :

K (orifice) = 0.09, and

K (nozzle) = 0.252

For the conical venturi meter used on tests at N.E.L., K will therefore be taken as 0.09.

It is now possible to calculate β for different values of f, taking m = 0.25 and $K_L = 2f$, by substitution in equations (V.21) and (V.25). These calculated values are as follows :

f	$\frac{1}{\sqrt{a}}$...	β'	β
0.011	0.3809	0.1826	0.9882
0.02	0.3847	0.1047	0.9883
0.03	0.3867	0.1886	0.9885

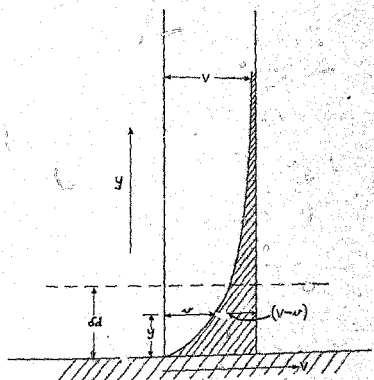

FIG. V.8 DISPLACEMENT THICKNESS OF THE BOUNDARY-LAYER

4. THE BOUNDARY-LAYER EFFECT

Variation of discharge coefficients for venturi meters could also be related to energy transformations within the instrument's boundary-layers. This remains a complex problem.

The author decided to allow for this effect by calculating the boundary-layer displacement thickness which, according to the Prandtl hypothesis, can be considered as an internal concentric thin-walled tube which decreases the theoretical effective cross-sectional flow area at the throat. Accordingly, $m' = \frac{A'_2}{A_1}$

where

m' = altered area ratio due to boundary-layer effect;

A'_2 = altered throat cross-sectional area, and

A_1 = upstream cross-sectional area.

Values were calculated for laminar and turbulent boundary-layers.

Referring to Fig. V.8 and writing the mathematical expression for δ_d (the displacement thickness) in accordance with its definition (for flow over a flat plate) :

$$V\delta_d = \int_0^{\delta} (V - v)\, dy$$

$$\therefore \delta_d = \int_0^{\delta} \left(1 - \frac{v}{V}\right) dy \qquad \ldots\ldots\ldots\ldots\ldots\ldots (V.30)$$

The velocity distribution in a boundary-layer follows the law :

$v = V F\left(\frac{y}{\delta}\right)$ where δ is the boundary-layer thickness.

Substituting this in equation (V.30) yields :

$$\delta_d = \int_0^1 \left[1 - F\left(\frac{y}{\delta}\right)\right] . d\left(\frac{y}{\delta}\right)$$

The exact solution for $F\left(\frac{y}{\delta}\right) = F(z)$ can be determined for a laminar boundary-layer, giving :

$$\delta_d = \int_0^1 \left[1 - F(z)\right] . dz = \frac{1.73}{\sqrt{R_L}} \qquad \ldots\ldots (V.31)$$

(R_L = Length Reynolds number)

Similarly it can be shown that the displacement thickness for a turbulent boundary-layer can be expressed in standard form as :

$$\delta_d = 0.046\, L\, (R_L)^{-0.2} \qquad \ldots\ldots\ldots\ldots\ldots (V.32)$$

The two possible conditions as formulated by equations (V.31) and (V.32) are to be treated separately.

4.1 Laminar boundary-layer

Substituting Hutton's value of $t = 1.3\ d$ in equation (V.31), and simplifying yields :

$t = 1.3\ d_2 = 2.6\ R_2$, where d_2 is the throat diameter.

$\therefore\ Re = \dfrac{1.3\ V \rho d_2}{\mu} = 1.3\ R_e$, where R_e is the throat Reynolds number.

$\therefore$ Equation (V.31) becomes :

$$\delta_d = \frac{1.73 \times 2.6\ R_2}{\sqrt{1.3\ R_e}} = 3.945\ (R_e)^{-0.5}$$

If the altered throat radius due to the displacement thickness is given by R_2', then :

$$R_2' = R_2 - \delta_d$$
$$= R_2 - 3.945\ R_2\ (R_e)^{-0.5}$$

$$\therefore\ \frac{\pi (R_2')^2}{\pi R_1^2} = \frac{\pi R_2^2}{\pi R_1^2}\left[1 - 3.945\ (R_e)^{-0.5}\right]^2$$

whence $m_A' = m\left[1 - 3.945\ (R_e)^{-0.5}\right]^2$ where

m_A' is the transformed area ratio.

4.2 Turbulent boundary-layer

Substituting $t = 1.3\ d$ in equation (V.32)

and simplifying yields :

$$\delta_d = 0.046 \times 2.6\, R_\lambda (1.3\, R_e)^{-0.2} \quad \text{whence,}$$

as before :

$$m'_t = m\left[1 - 0.11347\,(R_e)^{-0.2}\right]^2 \qquad \ldots\ldots\ldots(V.33)$$

where m'_t is the transformed area ratio. Hence m'_s and m'_t can be calculated for different values of R_e. The theoretical equations derived for C_d viz :

$$C_d = \sqrt{\frac{\delta(1 - m')^2}{\lambda_2 + K_L - \lambda_1 m'^2}} \quad \text{and}$$

$$C_d = \sqrt{\frac{\delta(1 - m')^2}{\lambda_2 - \lambda_1 m'^2}}$$

can now be evaluated on the strength of the following parameter values :

$\lambda_1 = 1 + 2.93\, f - 1.55\, f^{3/2}$ ..... (expressed in graphical form in Fig. V.3)

$\lambda_2 = 1.000$ (verified experimentally)

$K_L = 2f$

$\delta = 0.988$ (approximate theoretical value)

$m'_s = m\left[1 - 3.945(R_e)^{-0.5}\right]^2$

$m'_t = m\left[1 - 0.11347(R_e)^{-0.2}\right]^2$

Results are tabulated in Table V.1.

g = 0.9680

TABLE V.1

R_e (Throat)	2×10^4	5×10^4	1×10^5	2×10^5	3×10^5	4×10^5	5×10^5	6×10^5	7×10^5	5×10^6
R_p (Pipe)	1×10^4	2.5×10^4	5×10^4	1×10^5	1.5×10^5	2×10^5	2.5×10^5	3×10^5	3.5×10^5	2.5×10^6
f	0.0300	0.0253	0.0215	0.0180	0.0168	0.0161	0.0154	0.0149	0.0145	0.0110
λ_1	1.0825	1.0700	1.0590	1.0500	1.0460	1.0440	1.0429	1.0410	1.0400	1.0275
λ_2	1.0000	1.0000	1.0000	1.0000	1.0000	1.0000	1.0000	1.0000	1.0000	1.0000
$K_v = 2f$	0.0600	0.0506	0.0430	0.0360	0.0336	0.0322	0.0308	0.0298	0.0290	0.0220
m'_g	0.2363	0.2413	0.2438	0.2456	0.2464	0.2469	0.2472	0.2475	0.2477	0.2491
m'_t	0.2422	0.2436	0.2444	0.2451	0.2455	0.2457	0.2459	0.2461	0.2463	0.2474
C_d Laminar equ. (6.10)	0.9661	0.9703	0.9738	0.9770	0.9781	0.9788	0.9794	0.9799	0.9802	0.9835
C_d Turbulent equ. (6.10)	0.9661	0.9703	0.9738	0.9770	0.9781	0.9788	0.9794	0.9799	0.9802	0.9835
C_d Laminar equ. (6.11)	0.9965	0.9962	0.9958	956	0.9955	0.9954	0.9953	0.9953	0.9952	0.9949
C_d Turbulent equ. (6.11)	0.9964	0.9962	0.9958	0.9956	0.9955	0.9954	0.9953	0.9953	0.9953	0.9949
Hutton (m/m')	0.9720	0.9762	0.9797	0.9829	0.9840	0.9847	0.9853	0.9858	0.9861	0.9895

REFERENCES

1. Hall, G.W. 'Application of boundary-layer theory to explain some nozzle and venturi flow peculiarities'. Proc. Inst. Mech. Engrs. Vol. 173, No. 35, 1959 - Discussion on paper.

2. Spencer, E.A. and Thibessard, G. 'A comparative study of four classical venturi meters'. Flow measurement in closed conduits, Vol. 1, N.E.L. Proceedings of Symposium, Sept., 1960.

3. Engel, F.V.A. 'How to improve flow measurement accuracy of orifices, nozzles and venturi meters'. Flow measurement in closed conduits, Vol. 1, N.E.L. Proceedings of Symposium, Sept., 1960.

4. Winternitz, F.A.L. and Hopkins, D. 'Simple total pressure probes with spherical shields'. Instrument practice, October, 1950, Vol. 12, No. 10.

5. Winternitz, F.A.L. 'Effects of vibration on pitot tube readings'. The Engineer, London, March - April, 1956.

6. Kiel, G. 'Gesamtdruckger"at mit grosser Unempfindlichkeit gegen Schr"aganstr"omung' Luftfahrtforsch, 1935, 12(2).

7. Preston, J.H. and Norbury, J.F. 'The three-quarter radius flowmeter - a reassessment'. Flow measurement in closed conduits, Vol. 1, N.E.L. Proceedings of Symposium, Sept., 1960.

8. Stratford, B.S. and Ascough, J.C. 'A recent attempt at accurate airflow measurement by pitot static traverse'. Flow measurement in closed conduits, Vol. 1, N.E.L. Proceedings of Symposium, Sept., 1960.

9. Kalupaile, S. 'Significance of a component runner for the current meter method of flow measurement in closed conduits'. Vol. 1, N.E.L. Proceedings of Symposium, Sept., 1960.

10. Discussion on paper in Ref. (9), Flow measurement in closed conduits, Vol. 1, N.E.L. Proceedings of Symposium, Sept., 1960.

11. Benini, G. 'Researches on mutual interference and wall proximity effects on current meter readings'. Flow measurement in closed conduits, Vol. 1, N.E.L. Proceedings of Symposium, Sept., 1960.

12. Discussion on paper in Ref. (11). Flow measurements in closed conduits, Vol. 1, N.E.L. Proceedings of Symposium, Sept., 1960.

13. Coffin, J. 'First results concerning the effect of water temperature in the calibration tank'. Flow measurement in closed conduits, Vol. 1, N.E.L. Proceedings on Symposium, Sept., 1960.

14. Serpand, J. and Coffin, J. 'Influence of a current meter frame on the measurement of large discharges'. Flow measurement in closed conduits, Vol. 1, N.E.L. Proceedings on Symposium, Sept., 1960.

15. Discussion on paper in Ref. (14). Flow measurement in closed conduits, Vol. 1, N.E.L. Proceedings of Symposium, Sept., 1960.

16. Swiss Electrotechnical Committee : 'Regeln für Wasserturbinen'. S.E.V. Publication No. 178, 1947.

17. Neale, L.C. 'Some factors affecting the performance of venturi meters'. Flow measurement in closed conduits, Vol. 1, N.E.L. Proceedings of Symposium, Sept., 1960.

18. Stratford, B.S. and Accough, J.C. 'A recent attempt at accurate airflow measurement by pitot static traverse'. Flow measurement in closed conduits, Vol. 1, N.E.L. Proceedings of Symposium, Sept., 1960.

19. Discussion on paper in Ref. (3). Flow measurement in closed conduits, Vol. 1, N.E.L. Proceedings of Symposium, Sept., 1960.

20. Discussion on paper in Ref. (17). Flow measurement in closed conduits, Vol. 1, N.E.L. Proceedings of Symposium, Sept., 1960.

21. Schlag, A. 'Survey of studies of classical venturi meters at the University of Liège'. Ibid.

22. Rouse, H. and Abul-Fetouh, A.H. 'Characteristics of irrotational flow through axially symmetric orifices'. Trans. Amer. Soc. Mech. Engrs. Journal appl. Mech., 1950 17 (4).

23. Hutton, S.F. 'Prediction of venturi meter coefficients and their variation with roughness and age'. Proc. Instn. Civ. Engrs., 1954, 3 (3).

24. Discussion on paper in Ref. (2). Flow measurement in closed conduits, Vol. 1, N.E.L. Proceedings of Symposium, Sept., 1960.

25. Burch, G.E. and Wilson, T. 'The phlebomanometer - a new apparatus for direct measurement of venous pressure in large and small veins'. Journal Amer. Med. Assoc. 123, 1943.

26. Green, H.D. 'Circulatory system methods'. Glasser, O. (Ed.) Med. Phys. Chicago Year Book Publishers, 1950.

27. Stewart, G.N. 'The output of the heart in dogs'. Amer. Journ. of Physiology, No. 57, 1921.

28. Müller, A. 'Über die verwendung des Castelli - prinzips zur geschwindigkeitsmessung'. Helv. Physiol. Acta. 1954, (12).

29. Brannon, E.S. 'The cardiac output in man - a study of some of the errors in the method of right heart catheterization'. Amer. Journ. Physiology, No. 145, 1945 - 46.

30. Huston, W.B. 'Accuracy of airspeed measurements and flight calibration procedures'. N.A.C.A. Rep. No. 919, 1948.

31. Bamerle, H. 'Measuring instruments for pressure, velocity and direction measurements'. Ministry of Supply (A.V.A. Monograph), M.A.P. report and translation No. 982, 1947.

32. Bracey, W., Letko, W. and Russel, W.R. 'Windtunnel investigation of a number of total pressure tubes at high angles of attack'. N.A.C.A. Tech. Note No. 2331, 1951.

33. Winternitz, F.A.M. 'Cantilevered pitot cylinder' Engineer, Lond. 1955, 199 (5183).

34. Benedict, R.P. and Gunson, W.E. 'The directional pressure probe - cylindrical type'. Westinghouse Electric Corporation, Aviation Gas Turbine Division, Engineering Department Report No. A-1408, 1952.

35. Gagliardi, F.A. and Cedergren, G.A. 'The effect of hole geometry and angle of attack variation on the total pressure recovery of cylindrical pressure probes'. Westinghouse Electric Corporation, Aviation Gas Turbine Division, Engineering Department Report No. A-1413, 1951.

36. Getteiman, C.C. and Krause, N.L. 'Considerations entering into the selection of probes for pressure measurement in jet engines'. Instruments, 1953, 26 (9).

37. Peters, H. 'Druckmessung'. Handbuch der experimental physik, Vol. IV, Part I, 1931.

38. Markowski, S.J. and Moffat, E.M. 'Instrumentation for the development of aircraft power-plant components involving fluid flow'. E.A.E. Quart. Trans., 1948, 2(1).

39. Winternitz, F.A.L. and Hopkins, D. 'Simple shielded total pressure probes, of small dimensions and fast response.' Fluids report No. 54, N.E.L. East Kilbride, Glasgow, 1957.

40. Barna, S.P. 'Fluid mechanics for Engineers'. Butterworths Scientific Publications, London, 1957.

41. Russel, W.R., Gracy, W. and Letko, W. 'Wind-tunnel investigations of six shielded total pressure tubes at high angles of attack'. N.A.C.A. Tech. Note No. 2530, 1951.

42. Laufer, J. 'The structure of turbulence in fully developed pipe flow'. N.A.C.A. Rep. 1174, 1954.

43. Young, A.D. and Maas, J.N. 'The behaviour of a pitot-tube in a transverse total pressure gradient'. Aero. Res. Counc. Rep. & Memo. 1770, 1936.

44. McMillan, F.A. 'Experiments on pitot-tubes in shear flow'. Aero. Res. Counc. Rep. & Memo., 3028, 1957.

45. Livesey, J.L. 'The behaviour of transverse cylindrical and forward facing total pressure probes in transverse total pressure gradients'. J. Aero. Sci., 23 (10), 1956.

46. Davies, P.O.A.L. 'The behaviour of a pitot-tube in transverse shear'. *J. Fluid Mech.* 3 (1), 1958.

47. Oosthuizen, P.H. 'The measurement of velocity in incompressible turbulent flow'. *SAAS Journal*, July/August. Republic of South Africa, 1962.

48. Fuhrmann, G. 'Theoretische und experimentelle Untersuchungen an ballon modellen'. Dissertation Göttingen 1912.

49. [illegible] experimentelle untersuchung eine [illegible] strahlrohres bei hoher Reynoldszahl [illegible] Anhängen. 1929.

Allen, H.J. and Reeper, L.J. 'Piezometer investigations'. Trans. A.S.M.E., 54, MTH 1932.

51. Madau, A. 'Influence of type and dimensions of pressure boat on the recorded static pressure'. [illegible] 35. 1938.

[illegible] W.E. (Jnr.) 'An investigation of the influence of orifice geometry on static pressure measurements'. M.S. Thesis, M.I.T. 1949.

[illegible] A.K. 'On the effect of orifice size on static pressure reading at different Reynolds numbers'. Ingen.-Arch., 24(5), 1956. [Translation as N.A.C.A. Report No. T.P. 4[illegible] 1958].

Shaw, R. 'The influence of hole dimensions on static pressure measurements'. *J. Fluid Mech.*, Vol. 7, pt. 4, 1959.

55. Livesey, J.L., Jacks[illegible] and Southern, R.V. 'The static hole error problem'. Aircraft Engr., No. 396, Feb. 1960.

56. 'Fluid meters - their theory and application'. Report of A.S.M.E. Research Com. on Fluid Meters. 6th Ed., New York : Am. Soc. Mech. Engrs. 1959.

57. Shaw, R. 'The measurement of static pressure'. Aero. Res. Course. P.H., 2792, 1959.

58. King, W.C. 'Heat-transfer physical mechanism of anti-film sensing element used in static measurement'. Trans. Amer. Soc. Mech. Engrs., J. Basic Engng., 82 D (3), 1960.

59. Fage, A. 'On the static pressure in fully-developed turbulent flow'. Proc. of Roy. Soc. (A), Vol. 155, 1936.

60. Laufer, J. 'Some recent measurements in a two-dimensional turbulent channel'. Journ. of Aero. Sc., May, 1950.

61. Winternitz, F.A.L. 'Symposium on flow measurements in closed conduits' N.E.L. Scotland, 1966.

62. Ott, L.A. 'Theorie und Konstante-bestimmung des Hydrometrischen Flügels'. J. Springler, Berlin, 1925.

63. Lindquist, E. 'The calibration of current meters'. Tekniah. Tidskrift, Mechanik 10, Vol. 54, 1924.

64. Staus, A. 'Die genauigkeit von Flügelmessungen bei Wasserkraft-anlagen'. Berlin, Springer 1926.

65. Henn, W. 'Grundlagen der Wassermessung mit dem hydrometrischen Flügel'. Forschungsh. Ver. masch. Ing., 1937, 8 (385).

66. Ott, L.A. 'Observations on the use of current meters for precise flow measurement'. Trans. Amer. Soc. Mech. Engrs., 1935, 57 (5).

67. Müller, H.P. 'Rohrwassermessungen in Turbinenanlagen' Wasserwirtschaft, Stuttgart, 1954 - 55, 45 (8).

68. Robson, A.D. 'The effect of water temperature upon the calibration of a current meter'. Trans. Amer. Geophys. Un. 1954, 35 (4).

69. Winternitz, F.A.L., Hopkins, D., Whitaker, J. and McDonald, L. 'The simultaneous calibration of 13 small Ott current meters'. Instr. Pract., July 1955.

70. Dedon, H.R.A. 'A miniature current meter and free running rotary flowmeter'. Hydr. Res. Station, D.S.I.R., Wallingford, 1955.

71. Lindquist, E. 'On the errors of current meters'. Tekniak. Tidskrift, Mechanik 2, Vol. 57 1927.

72. Ower, E. 'The measurement of air flow'. Third Ed. Chapman & Hall. London, 1949.

73. O'Brain, M.P. and Folsom, R.G. 'Notes on the design of current meters'. Trans. Amer. Geoph. Un. Vol. 29 No. 2, April 1948.

74. Winternitz, F.A.L. and Fischl, C.F. 'A simplified integration technique for pipe flow measurement'. Water Power, 1957, 9 (6).

75. Nikuradse, J. 'The laws of turbulent flow in smooth pipes'. Forschungsh. Ver. dtsch. Ing. 1932. Ausgabe B, 3.

76. Nikuradse, J. 'The laws of fluid motion in rough pipes'. Forschungsh. Ver. dtsch. Ing. 1933. Ausgabe B, 4.

77. Ross, D. and Robertson, J.R. 'A superposition analysis of the turbulent boundary layer in an adverse pressure gradient'. J. Appl. Mech. 1951, 18.

78. Winternitz, F.A.L. and Fischl, C. 'The accuracy of the log linear methods for pipe flow integration'. M.E.L. Fluids report, East Kilbride, Glasgow, 1960.

79, 80. Winternitz, F.A.L. 'Comparison of flow measuring techniques at Kinlochleven hydro-electric station - preliminary and final tests'. M.E.L. fluids reports Nos. 59 and 65, East Kilbride, Glasgow, Oct., 1957 and Febr., 1958, respectively.

81. Leslie, W.H.P. 'An automatic digital recorder for impeller type current meters'. M.E.L. Fluids report No. 61. East Kilbride, Glasgow, Dec., 1957.

82. Greenaway, H.T. and Leslie, W.H.P. 'A multi-channel digital photographic recorder'. M.E.L. Fluids report No. 79, East Kilbride, Glasgow. May, 1959.

83. Greenaway, H.T., and Leslie, W.H.P. 'A digital time-generator and programmer'. M.E.L. Fluids report No. 80, East Kilbride, Glasgow, July, 1959.

84. Lever, E.H., Ritter, H., Woolfson, M. and Wright, C.T. 'The rotating-beam channel and 30-inch water tunnel at Admiralty Research Laboratories'. Proc. Instn. Mech. Engrs., London. 1957.

85. Hutton, S.P. 'Techniques for hydraulic machinery research'. Trans. Instn. Engrs. Shipb. Scotland, 1956 - 57. 100.

86. Winternitz, F.A.L. 'Comparative flow measurements at Fätschbach power station'. M.E.L. Fluids Report No. 92, Aug. 1960.

87. Hutton, S.P. 'The prediction of venturi meter coefficients and their variation with roughness and age'. Trans. Instn. Civ. Engrs. London, April, 1954, with discussion, Dec., 1954.

88. Herschel, Clemens 'The venturi meter' Trans. Amer. Soc. Civ. Engrs., Vol. 17, 1887, with discussion Vol. 18, 1888.

89. Gibson, A.H. 'Abnormal coefficients of the venturi meter' Min. Proc. Instn. Civ. Engrs. Vol. 199, 1914 - 1915, Part I.

90. Pardoe, W.S. 'Computation of the coefficient of discharge of venturi meters'. Engrng. News Rec., Vol. 8 No. 13, Sept., 1919.

91. 'Fluid meters, their theory and application'. Amer. Soc. Mech. Engrs. Res. publication, 1941, 4th Ed.

92. Engel, F.V.A. and Davies, A.J. 'Velocity profiles and flow of fluids through a contracted pipe flow'. The Engineer, Vol. 166, 1938.

93. Engel, F.V.A. 'Some problems of fluid-flow measuring devices'. Engineering, July, 1953.

94. Rivas, M.A. (jr.) and Shapiro, A.H. 'On the theory of discharge coefficients for rounded-[illegible]nce flowmeters and venturis'. Trans. A.S.M.E., A[illegible] 1956.

95. Spencer, E.A. and Hayward, A.T.J. 'The accurate calibration of flowmeters with water'. Trans. Soc. Inst. Tech. Vol. 9, No. 1, 1957.

96. Mahusmann, H. and Ehret, L. 'Der Strömungswiderstand in geraden, ebenen Spalt unter berücksichtigung der Einlaufverluste'. Jahrbuch der deutschen Luftfahrtforschung, 1942.

97. Pardoe, W.S. 'The effect of installation on the coefficients of venturi meters'. Trans. Amer. Soc. Mech. Engrs. Vol. 58, 1936.

98. Schlag, A. 'Experiences on venturi meters with convergent cones'. Revue générale de l' hydraulique, Paris, 1938, (24).

99. Spencer, E.A. 'A venturi meter with abnormal discharge coefficient'. N.E.L. Fluids publication No. 45, 1956.

100. Ferron, A.G. 'Velocity profile effects on the discharge coefficient of pressure differential meters' A.S.M.E. publication No. 62 - Hyd. - 8, June, 1962.

101. Coleman, E.P. 'The flow of fluids in a venturi tube' Trans. Amer. Soc. Mech. Engrs. Vol. 28, 1907.

102. Purdy, H.D. 'Model experiments for the design of a 60-inch water tunnel - part I - description of apparatus and test procedure', St. Anthony Falls Hydraulic Laboratory, Sept. 1948. Univ. of Minnesota, project report No. 10.

103. Foster, D.V. 'The performance of the 108 compressor fitted with low stagger-free vortex blading' N.E.L. project - unpublished.

104. Pardoe, W.S. 'The coefficient of Herschel-type cast iron venturi meters'. Trans. A.S.M.E., Vol. 67, July, 1945.

105. Taylor, G.I. 'Some recent developments in the study of turbulence'. Proc. 5th Inst. Congr. Appl. Mech. New York, 1938.

106. Schubauer, G.B. and Skramstad, H.K. 'Laminar boundary-layer oscillations and stability of laminar flow'. Nat. Bur. Stand. Res. Paper 1772, 1943.

107. Schlichting, H. 'Boundary-layer theory'. New York. McGraw Hill, 1962.

108 Miller, S.A. and Fejer, A.A. 'Transition phenomena in oscillating boundary-layer flows'. Journ. of Fluid Mech. Vol. 18, Part 3, March, 1964.

109. Witte, R. 'New Contributions to International Standardization in the field of flow Measurement' (In German). Brennst. - Wärmekr., 1953, 5(6).